Investigation of Nanodispersion in Polystyrene–Montmorillonite Nanocomposites by Solid-State NMR

SERGE BOURBIGOT,[1†] DAVID L. VANDERHART,[2] JEFFREY W. GILMAN,[1] WALID H. AWAD,[1] RICK D. DAVIS,[1] ALEXANDER B. MORGAN,[3] CHARLES A. WILKIE[4]

[1]Fire Science Division, Building and Fire Research Laboratory, National Institute of Standards and Technology, Gaithersburg, Maryland 20899

[2]Polymers Division, Materials Science and Engineering Laboratory, National Institute of Standards and Technology, Gaithersburg, Maryland 20899

[3]Chemical Sciences-Inorganic Materials Group, The Dow Chemical Company, Midland, Michigan 48674

[4]Department of Chemistry, Marquette University, P.O. Box 1881, Milwaukee, Wisconsin 53201

Received 10 February 2003; revised 7 August 2003; accepted 11 August 2003

ABSTRACT: Nanocomposites result from combinations of materials with vastly different properties in the nanometer scale. These materials exhibit many unique properties such as improved thermal stability, reduced flammability, and improved mechanical properties. Many of the properties associated with polymer–clay nanocomposites are a function of the extent of exfoliation of the individual clay sheets or the quality of the nanodispersion. This work demonstrates that solid-state NMR can be used to characterize, quantitatively, the nanodispersion of variously modified montmorillonite (MMT) clays in polystyrene (PS) matrices. The direct influence of the paramagnetic Fe^{3+}, embedded in the aluminosilicate layers of MMT, on polymer protons within about 1 nm from the clay surfaces creates relaxation sources, which, via spin diffusion, significantly shorten the overall proton longitudinal relaxation time (T_1^H). Deoxygenated samples

Guest Researcher from Laboratory GEMTEX of Ecole Nationale Supérieure des Arts et Industries Textiles (ENSAIT)

Correspondence to: J. W. Gilman (E-mail: jeffrey.gilman@nist.gov)

Journal of Polymer Science: Part B: Polymer Physics, Vol. 41, 3188–3213 (2003)

were used to avoid the particularly strong contribution to the T_1^H of PS from paramagnetic molecular oxygen. We used T_1^H as an indicator of the nanodispersion of the clay in PS. This approach correlated reasonably well with X-ray diffraction and transmission electron microscopy (TEM) data. A model for interpreting the saturation-recovery data is proposed such that two parameters relating to the dispersion can be extracted. The first parameter, *f*, is the fraction of the potentially available clay surface that has been transformed into polymer–clay interfaces. The second parameter, ϵ, is a relative measure of the homogeneity of the dispersion of these actual polymer–clay interfaces. Finally, a quick assay of T_1^H is reported for samples equilibrated with atmospheric oxygen. Included are these samples as well as 28 PS/MMT nanocomposite samples prepared by extrusion. These measurements are related to the development of high-throughput characterization techniques. This approach gives qualitative indications about dispersion; however, the more time-consuming analysis, of a few deoxygenated samples from this latter set, offers significantly greater insight into the clay dispersion. A second, probably superior, rapid-analysis method, applicable to oxygen-containing samples, is also demonstrated that should yield a reasonable estimate of the *f* parameter. Thus, for PS/MMT nanocomposites, one has the choice of a less complete NMR assay of dispersion that is significantly faster than TEM analysis, versus a slower and more complete NMR analysis with sample times comparable to TEM, information rivaling that of TEM, and a substantial advantage that this is a bulk characterization method. © 2003 Wiley Periodicals, Inc.* J Polym Sci Part B: Polym Phys 41: 3188–3213, 2003

INTRODUCTION

Interest in polymer–clay nanocomposite has increased significantly in recent years. The property improvements include better mechanical properties, better barrier properties, lower water absorption and reduced flammability.[1–6] To achieve these properties, mica-type layered silicates, such as montmorillonite (MMT), are generally dispersed at the nanoscale in the polymer to yield the so-called nanocomposite. The nanocomposite can be prepared via several routes including *in situ* polymerization,[7–9] bulk polymerization,[10] solution blending,[11,12] or melt blending in high-shear processing environments (extruder or other molding equipment).[13–16] All these routes are considered in this article.

Polymer–clay composites fall in three categories (Fig. 1).[13,17–19]

Microcomposites [Fig. 1(a)]

In microcomposites, the clay tactoids (finite stacks of clay platelets possessing their original platelet–platelet spacing) exist with no penetration of the polymer into the clay lamellae.

Exfoliated Composites [Fig. 1(b)]

In an exfoliated (or delaminated) nanocomposite, the individual clay layers are dispersed as single platelets into a continuous polymer matrix.

Intercalated Composites [Fig. 1(c)]

In an intercalated composite the insertion of polymer into the clay structure occurs to swell the spacing between platelets in a regular fashion, regardless of the clay-to-polymer ratio. Usually, however, an intercalated nanocomposite is normally interlayered by only a few molecular layers of polymer. Depending on the polymer–clay ratio, free polymer may or may not exist outside the clay regions.

Many of the properties associated with polymer–clay nanocomposites are a function of the extent of exfoliation of the individual clay sheets. Barrier properties, modulus, transparency, and toughness have all been shown[1] to be directly proportional to the degree of exfoliation or the quality of the nanodispersion.

From this brief description of polymer–clay nanocomposites it should be evident that techniques are needed to characterize the nanocomposite with resolution at the nanoscale. Traditionally this is done with transmission electron microscopy (TEM) and X-ray diffraction (XRD).[20] TEM and XRD provide essential information on the structure of the nanocomposite; TEM gives qualitative information, and extensive imaging is required to ensure a representative view of the whole material, whereas XRD allows quantification of changes in layered-silicate layer spacing. Other methods such as small-angle X-ray scattering[21] and rheological measurements[22,23] also serve to complement the XRD and TEM data.

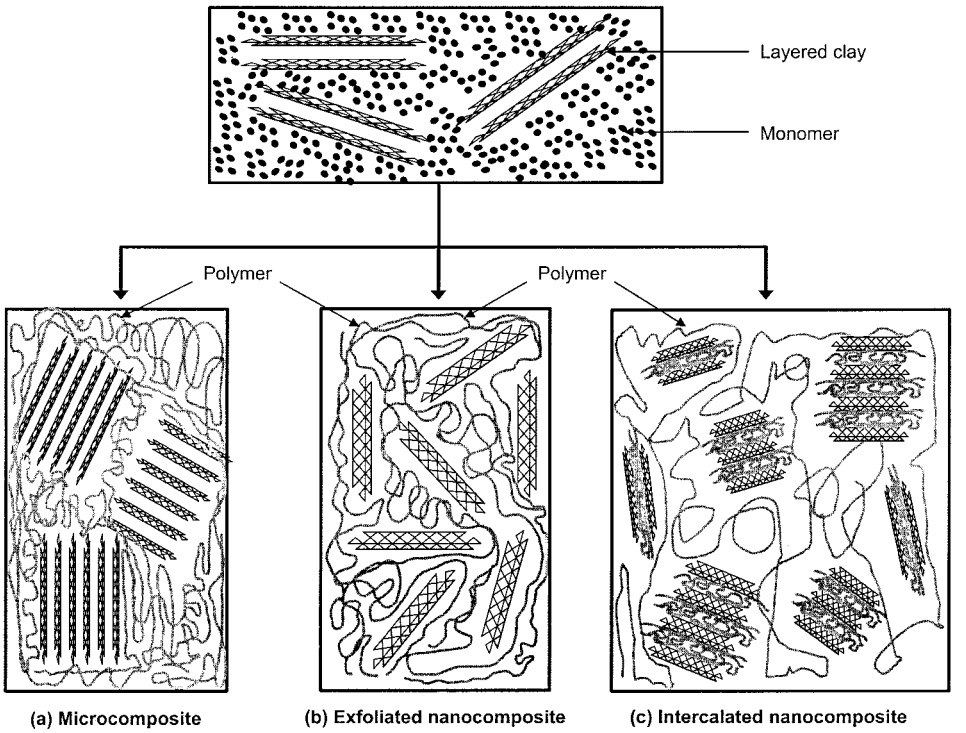

Figure 1. Illustration of (a) microcomposite, (b) exfoliated, and (c) intercalated polymer–clay nanocomposite morphologies. The nanocomposite was prepared by polymerization techniques from the monomer and from the organomodified layered clay (the fraction of clay is exaggerated for illustrative purposes).

New methods still need to be developed to complement these nanocomposite characterization techniques, especially methods that quantify the degree of nanodispersion of the layered silicate in the bulk polymer. An approach has been developed at the National Institute of Standards and Technology by VanderHart et al.[24–26] using solid-state nuclear magnetic resonance (NMR). The method is based on the T_1^H (proton longitudinal relaxation time) measurement. It uses two effects: (1) the paramagnetic character of this MMT that directly reduces the T_1^H of nearby protons and (2) spin diffusion, whereby this locally enhanced relaxation propagates to more distant protons. Up to now, this method has only been applied to polyamide-6 (PA-6) MMT nanocomposites exhibiting intercalated or exfoliated structures. NMR techniques are also useful in characterizing MMT dispersion and organo-MMT decomposition. It was suggested that the use of T_1^H, as a relative measure of MMT dispersion, could be applied to other polymer MMT nanocomposites. This article strives to demonstrate the application of this method to several polystyrene (PS) nanocomposites, which have been prepared via several routes. A significant difference between PA-6 and PS is the major role that molecular oxygen plays in determining T_1^H for PS, in contrast to the corresponding minor role it plays in PA-6. For deoxygenated samples, the intrinsic T_1^H of PS is very much longer than it is in PA-6, and this fact affords an opportunity to follow the clay-induced contribution to T_1^H for a longer time. Thus, more detailed information about the clay distribution is, in principle, available in PS. For this reason, we briefly revisit the modeling of spin diffusion in the presence of clay.

PS is a commodity polymer that is used in a number of commercial products. In 2001, PS was counted among the quantitatively most important thermoplastics and continues to be ranked in fourth place after polyethylene, polypropylene, and poly(vinyl chloride).[27] The main applications include packaging, extruded sheets, and consumer electronics. Improved mechanical properties with weight reduction, decreased vapor permeability, and low oxygen diffusion are the main development areas for packaging (foamed and foils packaging). Reduced flammability in the area of electronics is also required. Improvement

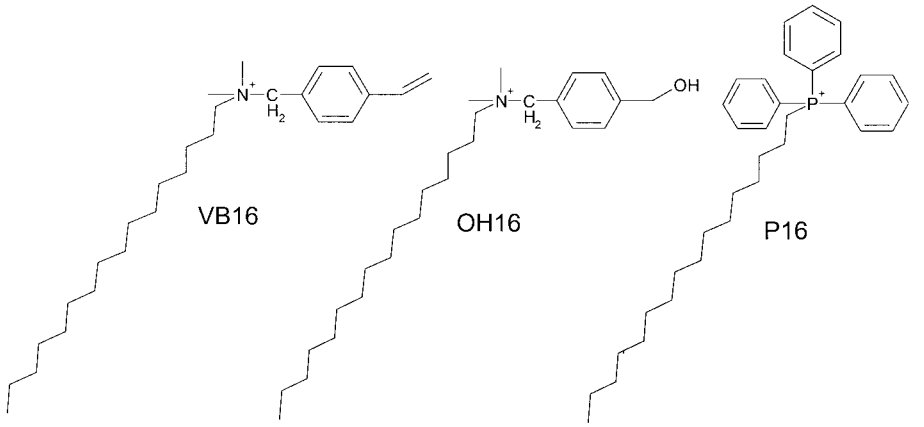

Figure 2. Structures of the salts used to prepare the organically modified clays VB16, OH16, and P16.

in these properties can be achieved with the nanocomposite approach. Only PS nanocomposites are considered in this study. The discussion of the preparation and mechanisms involved is beyond the scope of this article, but the reader may refer to refs. 1, 14, 15, and 28 to find useful information.

In our previous research,[10,12,15,28–33] several PS/MMT nanocomposites were prepared via different methods with MMT clay-exchanged with different organic modifiers. They exhibited exfoliated, intercalated, or mixed intercalated/exfoliated morphologies characterized by XRD and TEM. They also showed the unique combination of both improved mechanical properties and reduced flammability. They were used as model samples.

The first part of this article is devoted to modeling of the phenomenon of spin diffusion occurring during T_1^H measurement with the goals of providing two properties of the dispersion. The first property is the fraction, f, of the actual polymer–clay interfacial area, relative to the maximum possible polymer–clay interfacial area. The second property is a measure of the degree of homogeneity of the dispersion of actual polymer–clay surfaces. In the second part of this article, the results of characterizing the model PS nanocomposites by solid-state NMR (T_1^H measurement) are presented. The results are discussed and compared with XRD and TEM. The NMR method is also discussed in the context of high-throughput (or combinatorial) methods for examining polymer nanocomposites.[34] The latter samples were prepared with a twin-screw extruder and were characterized with NMR and TEM.

EXPERIMENTAL

Preparation of the Nanocomposites

The preparation of the nanocomposites used in this study has been described, and only a general description is given here. Several MMTs were used in making the nanocomposites. All MMTs originated from Southern Clay Products, Inc. (Gonzales, TX). Most of the modified MMTs used their sodium-MMT (Cloisite Na^+) as a precursor, whereas one of their already-modified MMTs, Cloisite 15A, was used as received. The organic modifier associated with the latter material was dimethyl-di-(hydrogenated tallow) ammonium.

The preparation of three other clays (Fig. 2) used in this study, namely, *N*,*N*-dimethyl-*n*-hexadecyl-(4-hydroxymethylbenzyl) ammonium chloride (OH16), *N*,*N*-dimethyl-*n*-hexadecyl-(4-vinylbenzyl) ammonium chloride (VB16), and *n*-hexadecyl triphenylphosphonium chloride (P16), have been described.[28] The preparation of the VB16, OH16, and P16 nanocomposites with styrene was accomplished by the bulk polymerization technique and is described in ref. 10. The concentration of the organo-modified MMT in PS was about 3 wt % (the weight percentage was used in this article and is identical to the mass-fraction percentage).

The preparation of the *N*-methyl-*N*,*N*-di(vinylbenzyl)octadecyl ammonium chloride (Fig. 3) and its ammonium clay, hereafter called DV, has been described in ref. 33. The preparation of the DV nanocomposite of styrene by the bulk polymerization technique was the same as above and has been described in refs. 10 and 33. The concentra-

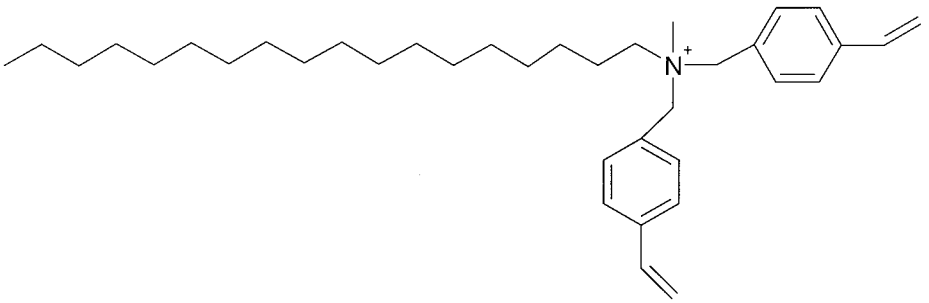

Figure 3. Structure of the salt used to prepare the organically modified clay DV.

tion of organo-modified MMT in PS was about 3 wt %.

The preparation of styryltropylium (Fig. 4) and its ammonium clay, hereafter called tropylium, has been described in ref. 29. The preparation of the PS tropylium nanocomposite from styrene has been realized by bulk and emulsion polymerization techniques.[31] The concentration of organo-modified MMT in PS was about 3 wt %.

Trialkylimidazolium salt derivatives were prepared with decyl and hexadecyl alkyl chains attached to the imidazolium through one of the nitrogens [1,2-dimethyl-3-hexadecylimidazolium chloride (DMHDIM) and 1,2-dimethyl-3-decylimidazolium chloride (DMDIM)] (Fig. 5). These imidazolium salts were used to prepare the corresponding treated MMT via standard ion-exchange procedures. These PS nanocomposites were prepared in a mini-twin-screw extruder (intermeshing, conical, DACA Corp.). Polymer (95 wt %) and trialkylimidazolium-treated MMT (5 wt %) were charged into the miniextruder and typically mixed at 21–31 rad/s (200–300 rpm) for 5 min at 180 °C.

The synthesis of the ammonium salt of the copolymer of styrene and vinylbenzyl chloride (COPS) and the ammonium salt of copolymer of methyl methacrylate and vinylbenzyl chloride (MAPS) (Fig. 6) have been described in ref. 30. The PS nanocomposites (PS supplied by Aldrich Chemical) were prepared by melt-blending in a Brabender Plasticorder at 60 rpm at 190 °C. The concentration of the organo-modified clays was about 15 wt %.

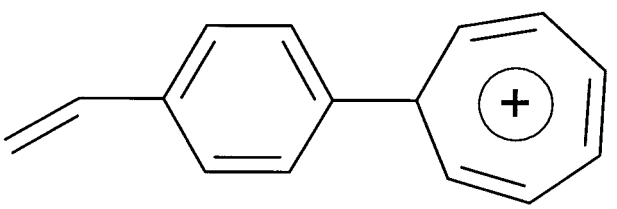

Figure 4. Styryltropylium cation. Cation should show aromatic character.

Samples containing organic-modified MMT (Cloisite 15A) in PS (Styron 663, Dow Chemical) were produced in our twin-screw extruder at various screw speeds [B&P, 19 mm, 25:1 L:D, feed rates (2–3) kg/h, feeding zone 170 °C, mixing zones (1–4) 190 °C]. Seven loadings (2, 3, 4, 5, 6, 7, and 8% mass fraction of Cloisite 15A) were prepared at five different screw speeds [250 rpm (26.2 rad/s), 300 rpm (31.4 rad/s), 350 rpm (36.7 rad/s), 400 rpm (41.9 rad/s), and 450 rpm (47.1 rad/s)]. These 28 runs were replicated four to five times each in a random fashion.

NMR Spectroscopy

Measurements were conducted with a Bruker Avance 300 spectrometer operating at 7.05 T. Proton spectra at 300 MHz were obtained with a 5-mm low-proton background CRAMPS[35] [combined rotation and magic-angle spinning (MAS)] probe manufactured by Doty Scientific of Columbia, SC. The MAS frequency was 2.5 kHz. Bloch decay spectra were obtained with a 90° pulse width of 1.5 μs and a 2 μs dead time.

We conducted our T_1^H measurements in two stages. In the first stage, we were focused on finding a method with the highest throughput; moreover, we did not yet appreciate the strong role that paramagnetic molecular oxygen played in determining the observed T_1^H's. However, the absorption of paramagnetic oxygen into aromatic polymers, such as polystyrene, causes a major shortening of T_1^H.[36,37] This effect becomes increasingly dominant with decreasing temperature. Thus, in the second stage, after we realized the role of oxygen, we remeasured the T_1^H's with de-

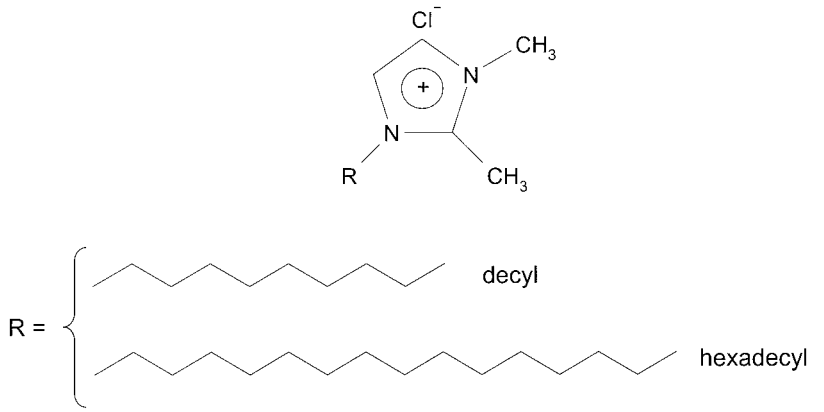

Figure 5. Structures of the imidazolium salts used in this work.

oxygenated samples. As mentioned, the inefficient relaxation of deoxygenated, unfilled PS enhances ones ability to obtain information about the dispersion of the paramagnetic clay because, as compared with oxygen-containing samples, one can follow the effects of the clay-induced relaxation for a longer period of time. Thus, in the second stage, we took more time looking at the details of the recovery curves and placed less emphasis on the high-throughput character of the measurement. We present data with both oxygen-containing and deoxygenated samples because we believe that both measurements produce correlations with other assays of dispersion quality. Our perspective is, however, that the most information can be obtained with deoxygenated PS samples.

T_1^H's of oxygen-containing samples were short (ca. 1–2 s) and were obtained with the inversion-recovery sequence with direct proton observation[38] in a ZrO_2 rotor. For purposes of time efficiency (high throughput), only the delay time (τ_{null}) was determined. The latter is the delay time where, after inversion, magnetization passes through zero on its way back to the Boltzmann equilibrium level. From τ_{null}, a lower limit for T_1^H was calculated via the relationship $T_1^H = \tau_{null}/\ln 2$. This relationship assumes full initial inversion of the magnetization and single-exponential recovery. The paramagnetic contribution to T_1^H originating from the MMT clay normally produces a slightly accelerated early decay relative to the typically exponential behavior seen at longer times; hence, this relationship systematically yields a lower limit to the T_1^H that would describe this longer time behavior. In any case, all of the samples had equilibrated with O_2 and had aged for at least 1 month. Standard uncertainties for τ_{null} measurements are ±2.5% of the given value.

Deoxygenated granular samples were prepared by pumping at high vacuum for 1 h at 90 °C in 5-mm o.d. glass tubes and sealing the tubes. T_1^H recovery curves were then measured with the saturation-recovery sequence with direct proton observation.[38] Three closely spaced 90° pulses accomplished the saturation. This sequence was

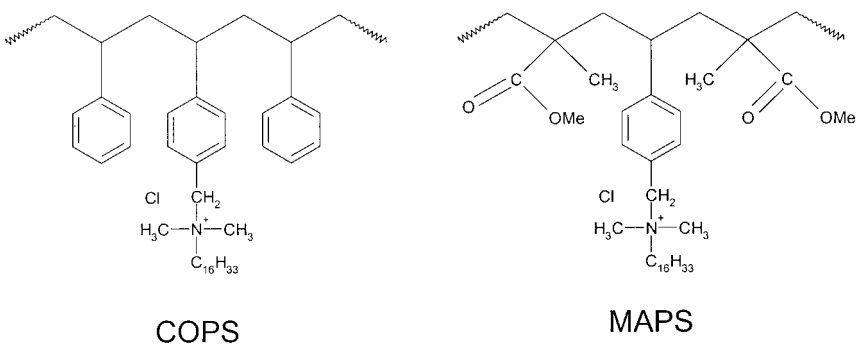

Figure 6. Structures of the COPS and MAPS salts used in this work.

preferred over the inversion-recovery sequence to minimize the number of experiments that would require long relaxation delays (five times the longest T_1^H). As a semiempirical approach to analysis, these saturation-recovery curves were fit to a two-exponential equation according to

$$M(t) = M_{0s} \cdot (1 - e^{-t/T_{1s}^H}) + M_{0l} \cdot (1 - e^{-t/T_{1l}^H}) \quad (1)$$

where $M(t)$ is the magnetization at time t; M_{0s} and M_{0l} are the magnetization of the short and long components, respectively, and; T_{1s}^H and T_{1l}^H are the proton longitudinal relaxation times of the short and long components, respectively. The physical meaning of these components is discussed subsequently. The equation was fit with the commercial program TableCurve2D of Jandel Scientific with a standard least-squares minimization (Gaussian elimination). The accuracy of the fit was evaluated by an analysis of residuals in a 95% confidence domain. All fitted values of T_{1l}^H and T_{1s}^H had 3 and 5% standard uncertainties, respectively. Corresponding standard uncertainties for the two M_0's were typically less than 5%.

TEM

All samples except for PS/Cloisite 15A nanocomposite series were ultramicrotomed with a diamond knife on a Leica Ultracut UCT microtome to give sections with a nominal thickness of 70 nm. The sections were transferred from water (room temperature) or dry conditions (−110 °C) to carbon-coated Cu grids of 200 mesh. Bright-field TEM images of nanocomposites were obtained at 120 kV under low-dose conditions with a Philips 400T electron microscope, with Kodak SO-161 film. Low-magnification images were taken at 2800× and 10,000×. High-magnification images were taken at 28,000× and 60,000×. The materials were sampled by taking several images of various magnifications over two to three sections per grid to ensure that analysis was based on a representative region of the sample.

In the case of PS/Cloisite 15A nanocomposite series, materials were thin-sectioned at −90 °C with a Reichert Jung Ultracut E ultramicrotome equipped with an FC-4E cryo-chamber. Sections were collected on a copper grid and examined with a Philips CM-12 TEM (Serial # D769) running at an accelerating voltage of 120 kV. Images were recorded digitally with a Gatan Multiscan charged coupling device camera, Model 749.

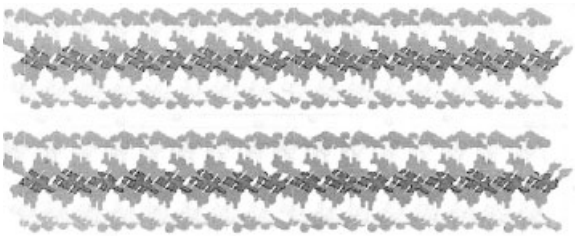

Figure 7. Molecular representation of sodium MMT, showing two aluminosilicate layers with the Na^+ cations in the interlayer gap or gallery. The octahedral alumina layer (central layer) is surrounded by oxygen atoms. The outside layers consist of silicate tetrahedra (from ref. 15).

Thermogravimetric Analysis (TGA)

TGA was carried out with a TA Instruments Simultaneous TGA-DTA (SDT 2960) at 10 °C/min from 25 to 800 °C in air flow (100 cm^3/min). Samples of 5–10 mg each were put in open alumina pans. Typically, three replicates were run for each sample, and the mean was reported. Both the onset (5% mass-fraction loss) and peak mass-loss rate had an uncertainty of 1.2 °C (2σ). The final residue of PS/MMT nanocomposites was used to establish the concentration of inorganic MMT in the samples. These values were used in the calculation of the degree of homogeneity.

SPIN-DIFFUSION MODELING IN POLYMER/MMT NANOCOMPOSITES

MMT clay is a smectite, layered aluminosilicate in which each platelike layer is about 1.0 nm thick and from 50 to 100 nm in lateral dimension. The surfaces of the layer are mainly made up of silica tetrahedral, whereas the central plane of the layer contains octrahedrally coordinated Al^{3+} with frequent nonstoichiometric substitutions, where an Al^{3+} are replaced by Mg^{2+} and sometimes by Fe^{3+} (Fig. 7).[39] Mg^{2+} substitution leaves an embedded negative charge in the clay that must be neutralized with a cation at the surface. Usually, this is an inorganic cation like Na^+, but one can also introduce an organic cation like a tetrasubstituted ammonium ion to serve as an ionically bound organic modifier.

In this distorted octahedral environment, Fe^{3+} is strongly paramagnetic (S = 5/2). The spin-exchange interaction between the unpaired electrons on different Fe atoms produces magnetic fluctuations in the vicinity of the proton Larmor

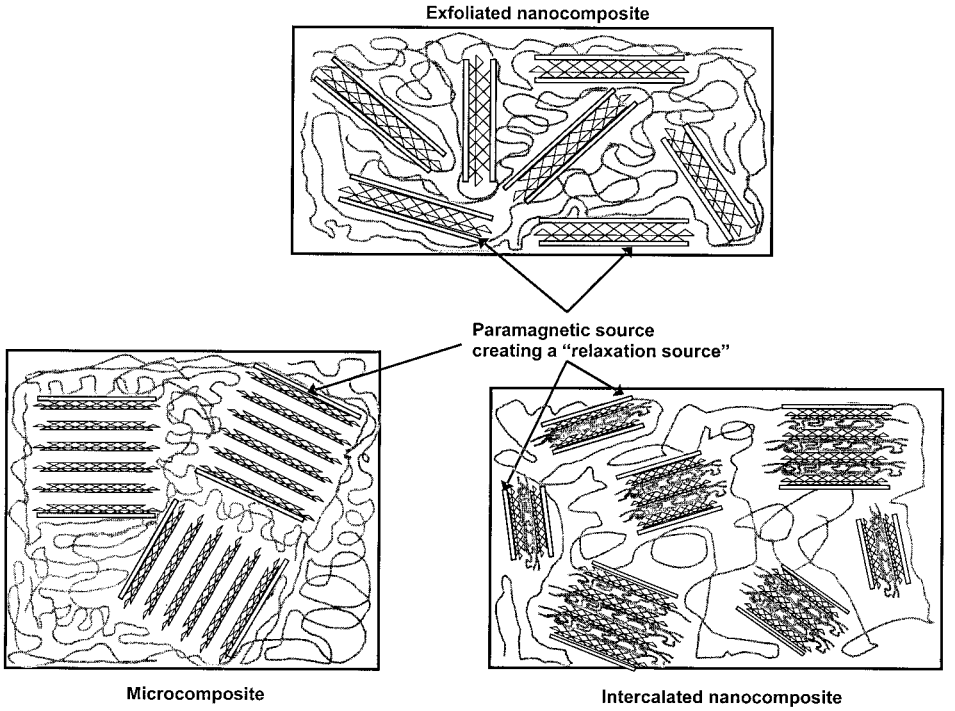

Figure 8. View of the paramagnetic source because of Fe^{3+} embedded in the MMT platelets creating relaxation sources in different morphologies of nanocomposite. The clay concentrations in our samples were much lower than pictured here.

frequency (the frequency at which spins are processing) for protons. This fact is important because the longitudinal relaxation of protons, T_1^H, within about 1.0 nm of the clay surface is directly shortened. The range of the direct relaxation is limited by the fact that the relaxation of a proton by a Fe^{3+} site near a clay surface depends on the inverse sixth power of the internuclear distance.[40] This local, paramagnetically induced relaxation influences the overall measured T_1^H because spin diffusion allows this relaxation mechanism to propagate into the bulk of the polymer. The extent of this effect on T_1^H depends on both the Fe and MMT concentration, and most importantly, on the average distance between nearest polymer/MMT interfaces. Clay layers having no polymer interfaces, to a good approximation, do not influence T_1^H. Thus, the better the dispersion of single MMT layers, the shorter is the average T_1^H. T_1^H measurements can therefore be used to probe the dispersion at the nanoscale of MMT in the polymer. When we speak of T_1^H in an average sense, we are not claiming that all nuclei relax exponentially, nor are we suggesting that all spins relax at the same rate. Indeed, those spins that are close to a clay–polymer interface will experience a rather rapid initial decay, whereas those that are far away from a clay–polymer interface will have a slower initial decay rate. If all spins are affected by the presence of the paramagnetic clay, none of their relaxation profiles is strictly exponential; hence, describing decays by T_1^H's is an approximation. Thus, if paramagnetic relaxation is active in these nanocomposites, we use multiexponential fits and interpret these fits in a strictly semiempirical way. However, at longer times it is expected that in a system with good dispersion the long-time portion of the decays of all spins is exponential with a single T_1^H. Thus, it makes sense to analyze these curves with multiple T_1^H's to extract the longer T_1^H.

A schematic view of this effect is presented on Figure 8. The initial proof of the effectiveness of the NMR technique was demonstrated in PA-6/MMT nanocomposites.[26] The point of this section is to use the previously introduced[26] spin-diffusion model to describe the paramagnetically induced relaxation of MMT platelets in these PS nanocomposite structures. We will, however, feature different aspects of the model calculation that are more appropriate to these PS nanocomposites.

Proton spin-diffusion[41] data yield morphological information over dimensions whose upper limit depends on the intrinsic T_1^H. For our particular case, where T_1^H of pure PS is about 39 s, the range is about 2–400 nm. If we consider the phenomenon of spin diffusion in the case of polymer/MMT nanocomposites, we have a mechanism for propagating the enhanced relaxation to protons much more distant from the clay surface. We will model the T_1^H behavior measured in an inversion-recovery or saturation-recovery experiment considering the evolution of spin magnetization in a one-dimensional model with finite sources (clay platelets) and a finite source (polymer).

The fundamental equation describing the behavior of the Zeeman component of spin magnetization for a system with uniform proton density under the influence of both spin diffusion[41] and longitudinal relaxation is given by the Fick's law (eq 2) (see ref. 42 for a full discussion on proton spin diffusion applied to polymer morphologies)

$$\frac{\partial P(r,t)}{\partial t} = \mathrm{div}\{D \cdot \overrightarrow{\mathrm{grad}}[P(r,t)]\} + \frac{P_0 - P(r,t)}{T_1^H} \quad (2)$$

where $P(r,t)$ is the ensemble-averaged Zeeman polarization per spin, averaged over morphologically corresponding positions r and spin-diffusion time t; P_0 is the polarization per spin associated with Boltzmann equilibrium; and D is the spin-diffusion coefficient (assumed to be a scalar and constant). The total spin magnetization, $M(t)$, which is proportional to the NMR signal intensity, can be obtained by integrating $P(r,t)$ over the region of interest Ω:

$$M(t) = \int_\Omega P(r,t) \cdot dr \quad (3)$$

These two equations (eqs 2 and 3) can be applied to simulate spin diffusion in spin–lattice relaxation experiments by choosing the appropriate initial conditions (T_1^H is assumed as a constant in a region Ω in the following).

Our first approach to simulate a spin–lattice relaxation experiment is to consider a very well exfoliated system (perfectly stratified system). The model[26] consisted of two distinct domains (Fig. 9)—the region of the paramagnetic source and the region of the polymer (PS). To simplify the calculation, the assumptions are as follows: (1) the intrinsic T_1^H for the polymer layers in the nanocomposite is the spin-diffusion averaged T_1^H of the pure polymer; (2) MMT platelets are parallel to one another and equally spaced (Δ is the platelet–platelet spacing); and (3) the paramagnetic influence of the Fe in the clay is replaced and mimicked by a fast-relaxing thin layer of PS (we assume 0.4 nm as was done in the case PA-6 nanocomposite[26]) whose protons are in spin-diffusion contact with the rest of the polymer. The choice of 0.4 nm, rather than 1.0 nm, is somewhat arbitrary. By modeling the problem as we have done, all we are creating is a relaxation source whose somewhat arbitrary width is tightly coupled to the relaxation time $(T_1^H)_s$ assigned to this region in any fitting procedure.

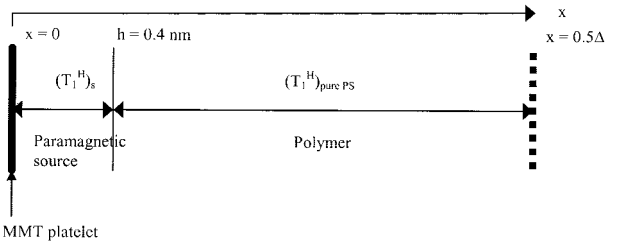

Figure 9. One-dimensional model simulating a perfect stratified system. Two regions can be distinguished: a narrow region experiencing direct paramagnetically induced relaxation and a much broader region experiencing only indirect paramagnetically induced relaxation. There is no polarization transport across the clay surface nor is there transport across the boundary at 0.5Δ because of assumed symmetry.

With a spin-diffusion coefficient D = 0.6 nm^2/ms for the two regions,[42,43] we model both the spin diffusion and the relaxation during a typical saturation-recovery experiment. Before starting any computation, we need to estimate Δ, the platelet–platelet spacing. Our model assumes a regular, repeating lamellar structure of alternating clay and PS; then, the spacing can be calculated by $\Delta = \left(\frac{V_{clay}}{V_{tot} \cdot d_{clay}}\right)^{-1}$ where V_{clay} and V_{tot} are, respectively, the fractional volume occupied by the clay and the total volume in the nanocomposite. Hence, with a thickness, d_{clay}, of 1.0 nm for each clay layer, the densities of ρ_{PS} = 1.04 g/cm^3 for PS and ρ_{clay} = 2.86 g/cm^3 for MMT, and mass fractions are between 2 and 3% of MMT (from TGA combustion residues, intentionally neglecting contributions from the organic modifier); then the spacing Δ falls between 86 and 136 nm for the samples considered herein. We illustrate some of the properties of the model calculation and take Δ

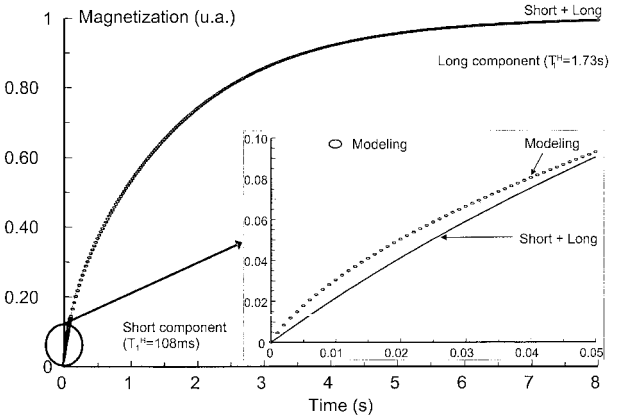

Figure 10. Evolution of the magnetization during a saturation-recovery experiment. The dotted curve (modeling) is the curve resulting from the one-dimensional model. It is simulated with a biexponential fitting curve containing a short and a long component.

= 100 nm, T_1^H (of the pure polymer) = 39 s and $(T_1^H)_s$ = 2 ms, where $(T_1^H)_s$ is the relaxation time in the 0.4-nm interface layer.

Finite-element methods were used to solve the equations (eqs 2 and 3) over the two regions. This computation simulated the total spin magnetization versus time for a spin–lattice relaxation experiment with the values discussed above. This calculated curve is depicted in Figure 10. We then attempted a biexponential fit (see Experimental) that gave a short component with a T_{1s}^H of 108 ms and a long one with a T_{1l}^H of 1.73 s. As expected, the fit was excellent at longer times where steady-state polarization gradients had a chance to develop. However, a closer look at earlier times shows that the biexponential approximation fits poorly for $0 < t < 50$ ms. This aspect is subsequently because we argue that the early slope is an important parameter.

The model calculation demonstrated that relaxation sources at the polymer–clay interfaces shortened the overall T_1^H from 39 s for pure PS to 1.7 s for this well-exfoliated model. Thus, we can expect a large influence of the nanodispersion of MMT on T_1^H. However, the use of a biexponential fit serves only to capture the T_1^H at longer times; this fit lacks adequate precision in duplicating the initial slope.

In the following, we introduce two concepts for analyzing the experimental recovery curves under the assumption that the concentration of clay (inorganic part) is independently known. These concepts are intended to answer two separate questions about the clay dispersion, namely, what fraction of the clay layers become dispersed into the polymer and what is the homogeneity of the distribution of those polymer–clay surfaces that were formed. An important perspective to introduce, which we expand on subsequently, is that this method holds significant bias against small Δ's in the range of a few nanometers. In other words, this method is not expected to offer any accurate count of surfaces that are part of an intercalated structure housing polymer layers only a few nanometers thick. This method is much more suited to evaluate exfoliation rather than intercalation.

For the first concept, we argue that in a plot of recovering magnetization versus the square root of time, the initial slope, defined between 5 and 50 ms, and corrected for the contribution from the intrinsic T_1^H of PS, is nearly proportional to the total polymer–clay interfacial area. We then further assume that the relevant proportionality constant can be inferred from a proper calibration sample. Then this experimentally determined interfacial area, combined with knowledge of the clay concentration, will allow one to determine f, the fraction of effective polymer–clay interfacial area that did form relative to the maximum amount that could have formed. Also, from the initial slope of the calibration sample, one can establish $(T_1^H)_s$, the intrinsic relaxation time assigned to the 0.4-nm-wide interfacial region.

The second concept is that the long T_1^H, that is, T_{1l}^H, obtained from the biexponential fit to the experimental data can be matched, with our model calculation, to an apparent mean spacing, Δ_{app}, between clay–polymer interfaces. That is, after proper calibration, D and $(T_1^H)_s$ are fixed in the calculation, thereby leaving Δ_{app} as the only variable that defines the long T_1^H of the final slope. However, because we have also determined f and presumably know the clay concentration, we can also calculate an idealized spacing, Δ_f, corresponding to an idealized dispersion of the actual interfacial area. Then, the ratio of Δ_f/Δ_{app} will be a qualitative relative measure of the homogeneity of the dispersion of the actual surface area, that is, ratios significantly less than unity imply poor dispersion of the available interfaces.

A successful analysis of recovery curves in the way just outlined also depends on there being only two contributions to T_1^H relaxation, namely, the intrinsic, mainly dipolar relaxation of glassy PS and the paramagnetic contribution from the clay. To the extent that the sample also contains other materials, for example, excess solvent, re-

sidual monomers, and mobile contaminants, which have short T_1^H's and are well distributed in the PS lattice, one can be misled about the clay dispersion if these contributions are not also factored in.

For the purposes of extracting the parameter, f, from the initial slope, we justify the definition of the initial slope partly from a theoretical point of view and partly from a practical visual point of view on the basis of the model calculation of Figure 10. Theoretically, if spin diffusion from paramagnetic surfaces were the only mechanism for causing relaxation, then the change in magnetization should be linear versus the square root of time,[42,44] provided that the relaxation rate at the surface is infinitely fast. Furthermore, the initial slope will be directly proportional to surface area for $t < (\Delta^2/8D)$. In other words, if the surface represents a relaxation source that is maintained at a fixed (e.g., Boltzmann) polarization and the PS protons have a fixed but different initial polarization, then this relationship holds until the diffusion fronts that are moving away from the paramagnetic interfaces encounter other fronts approaching from nearby interfaces. In our case, several of these conditions are violated. First, there is no initial polarization gradient between surface and bulk protons. Second, the relaxation source does not have infinite capacity; rather, a typical average T_1^H near the interface would be about 2 ms. Third, there is a competing but weak T_1^H of 39 s for the pure PS. In the case under consideration, it takes on the order of a few times $(T_1^H)_s$ to generate a significant polarization gradient near the polymer–clay interfaces, and, even then, the average polarization at the surface changes with time. Strictly speaking, for the initial conditions of our experiment, we do not expect an initial slope that is linear in $t^{1/2}$. In Figure 11 the curves that appeared in Figure 10 are replotted versus $t^{1/2}$.

The behavior of the calculated curve (Fig. 11) is, as expected, nonlinear at the very earliest times because of the lack of an initial polarization gradient. However, for the range 5 ms $< t <$ 50 ms (0.07 $s^{1/2} < t^{1/2} <$ 0.22 $s^{1/2}$), one has a near-linear slope even though that the polarization level near the interface is not constant. At the same time, the biexponential fit, which also did not duplicate well the initial slope in Figure 10, is quite nonlinear in this plot. The fact that all the protons decay with an intrinsic T_1^H of 39 s is easy to correct for in Figure 11, that is, the growth from this term is just $1 - \exp(-t/39\text{ s}) \approx t/39$ s. In

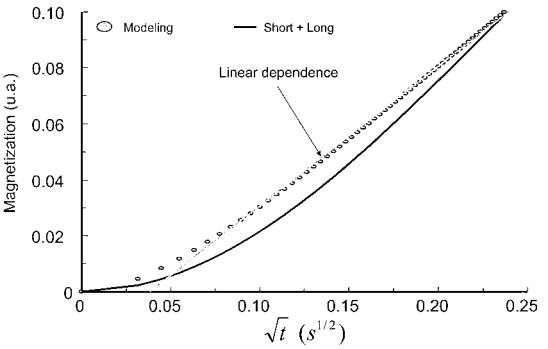

Figure 11. Magnetization versus the square root of the time calculated with the one-dimensional model assuming a perfect exfoliated system with its fit with a biexponential.

Figure 11, this is a negligible, parabolic correction whose amplitude is only 0.0012 at $t^{1/2} = 0.22$ $s^{1/2}$. In other words, spin diffusion from the paramagnetic surfaces is very dominant at early times in these deoxygenated PS nanocomposites. The fact that the model calculation has a nearly linear slope over the 5–50-ms range suggests that we can use such a plot, over the same range of time, to establish a T_1^H-corrected slope that is proportional to the surface area. The only qualifier comes from the condition that linearity is expected to fail for those galleries whose separation is sufficiently small. It is easiest to illustrate this point visually because there is no neat cutoff where galleries below a certain value contribute nothing, whereas those above contribute fully. In Figure 12, we used the results from our model calculation to plot the relative contributions to the initial slope from a fixed polymer–clay interface area whose magnitude corresponded to an average gallery spacing of 100 nm, assuming equidistant layering of the interfaces. However, instead of having 100-nm galleries, the gallery spacing was small and variable (with a large portion of the sample devoid of clay). We also fixed $(T_1^H)_s$ at 2.5 ms (the experimental justification of this value is given), in keeping with the value that we establish as being appropriate for these nanocomposites.

Figure 12 demonstrates that as the gallery spacing decreases, two things happen. First, curves have smaller values at $t = 50$ ms. Second, curves exhibit more downward curvature at longer times. The slope reaches an asymptote for larger Δ, represented by $\Delta = 32$ nm. From Figure 12, one concludes that even for $\Delta = 8$ nm, the slope is quite linear, although its contribution is

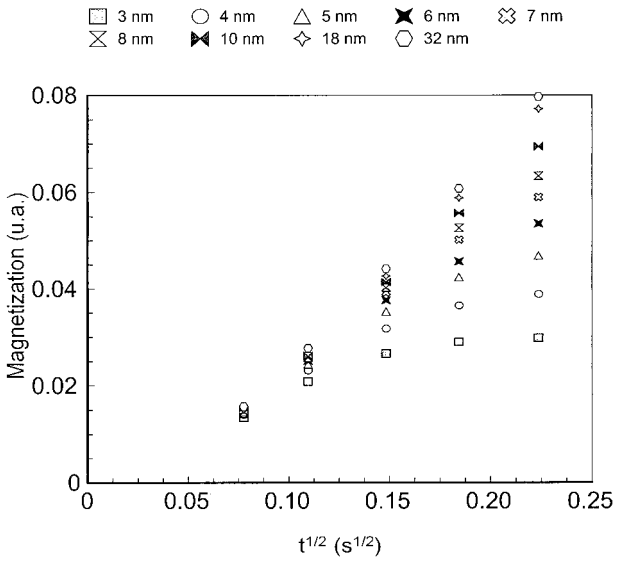

Figure 12. Simulated magnetization versus the square root of the time for different gallery spacings.

reduced by about 25%. Thus, if in a real sample the smallest gallery were 8 nm thick, the f value obtained from the initial slope would be slightly underestimated. However, for Δ's showing asymptotic slopes (Δ > 20 nm), curvature is slightly upward (see Fig. 11); thus, given a distribution of Δ in any sample, one could tolerate a minor amount of galleries smaller than 8 nm and still have a net linear slope. If one observes downward curvature experimentally, it is a sure sign that a significant population of the Δ distribution has Δ's that are 5 nm or less, and it is a warning that f might be significantly underestimated. Thus, a linear experimental slope, as a measure of the polymer–clay surface area, is most reliable when the minimum Δ in a sample is about 10 nm. A corollary is that when Δ > 10 nm, the slope, corrected for the small contributions from the 39-s PS T_1^H, is nearly linear in polymer–clay interface area and it is linear when Δ is large enough to exhibit the asymptotic slope. Most of the experimental data are linear, within experimental error, in the 5–50-ms range.

A comment, intended to help justify the plotting of data versus $t^{1/2}$, is the following: We recognize that from a mathematical point of view, this diffusion problem, with the representative parameters defined [e.g., Δ, $(T_1^H)_s$, etc.] is typically neither in the relaxation-limited domain (where diffusion is so fast that after each relaxation event near the interface, and the polarization is fully distributed throughout the system) nor is it in the diffusion-limited regime (where relaxation is faster than the elementary time step for diffusive processes). Given that relaxation near the interface is occurring on the 2-ms timescale, the time required to distribute polarization over a 100-nm gallery is about 2 s, and the timescale for the elementary diffusive process to move up or down a chain or between chains is the order of 0.1 ms, it is clear that this problem is much closer to the diffusion-limited case than to the relaxation-limited case. Hence, it makes sense that the $t^{1/2}$ dependence of the initial slope that characterizes the diffusion-limited domain is a better descriptor than the exponential dependence characteristic of the relaxation-limited domain. At the same time, as a gallery thins down toward a few nanometers, relaxation within that gallery approaches the relaxation-limited domain.

It is important to recognize that the measurement of f is not very dependent on the distribution of Δ values unless a significant portion of that distribution has Δ's less than 10 nm. Thus, it is a pretty robust and model-independent quantity. Another attractive feature with the initial slope to determine f is that one is obtaining these data over times shorter as compared with even the shortest possible proton dipolar relaxation times (175–250 ms at 7.05 T).[45] Thus, for example, interferences from 2% of some mobile, fast-relaxing contaminant, would contribute a maximum additional magnetization of 0.6% at 50 ms. Although this is not trivial, some of the observed paramagnetic effects are an order of magnitude larger.

RESULTS AND DISCUSSION

This section is organized in a way that separates the discussion of samples in terms of initial slopes (related to fractional surface areas, f) from the discussion of T_{1l}^H (related to the homogeneity of clay dispersion). We do this mainly because the slope gives the more powerful and quantitative measure of dispersion, unless the Δ distribution includes many small galleries. Thus, it is instructive to explore the level of information resident in the f values because we believe one would often have adequate reason to screen out a process or an organic modifier on the basis of a low f value alone. Moreover, the initial slope is less prone to experimental problems having to do with contamination with mobile species or assumptions about how average gallery spacings should depend on the polymer–clay interface area. Additionally, in

terms of experimental time spent acquiring data, one can collect data for the initial slopes relatively quickly (≈15 min) if one is interested in more rapid analysis.

Following this discussion, we take up the subject of T_{1l}^{H} and the homogeneity of the clay distribution for these samples. This analysis is more qualitative, depends more on assumptions about calculating realistic average Δ's, and is probably less useful as a screening tool. However, particularly for those cases where there are numerous, small galleries, this parameter offers important insight into dispersion. Measurement of T_{1l}^{H} also takes on importance when one wishes to verify that a well-exfoliated sample ($f \approx 1$) actually has its platelets evenly distributed.

Finally, we take a brief look at our early attempt to use oxygenated samples, with a quick measure of T_1^H, in a high-throughput application where the goal was to optimize process parameters (residence time in an extruder and MMT loading) in a physical blending of PS and clay. These are the data that we took before we appreciated the important role of oxygen in determining T_1^H. Qualitative correlations with clay dispersion were deduced from these data; however, we will show via subsequent examination of a subset of these samples as deoxygenated materials, that one gives up a lot of information with the former approach.

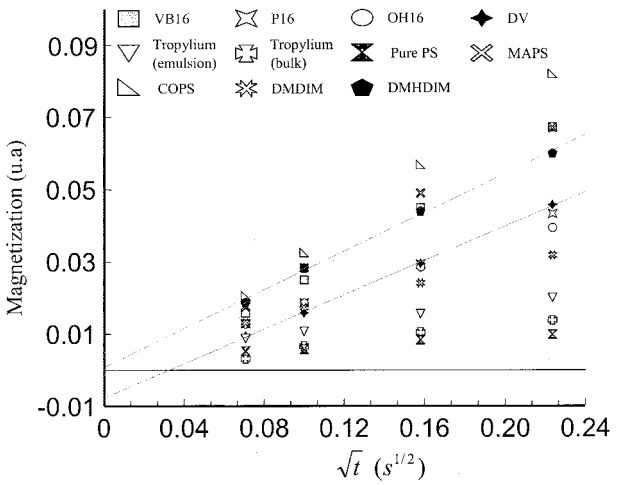

Figure 13. Magnetization from saturation-recovery experiment versus the square root of the time of deoxygenated PS/MMT nanocomposites.

Figure 14. TEM pictures of PS-VB16 nanocomposites exhibiting an exfoliated structure (from ref. 28).

Estimation of the Fraction of Effective Polymer–Clay Interfacial Area in Model PS/MMT Nanocomposites

Our theoretical approach has shown that the first part (at the very earliest times) of the total spin-magnetization curve is related to the polymer–clay interfacial area available in the matrix, or in other words, the initial slope of the curve is proportional to the polymer–clay interface concentration provided that the Δ distribution exhibits only minor populations with $\Delta < 8$ nm. Curves of Figure 13 determine that the experimental magnetizations exhibit linear dependence versus the square root of the time (5 ms $< t <$ 50 ms). They show that the samples exhibit distinguishable slopes that range more widely than the clay loadings; thus, it can be expected that the nanocomposites should exhibit different degrees of nanomixing.

To calculate the fraction of the effective polymer–clay interfacial area, f, from the initial slopes, we need to choose a reference sample that exhibits a fully exfoliated structure. The best can-

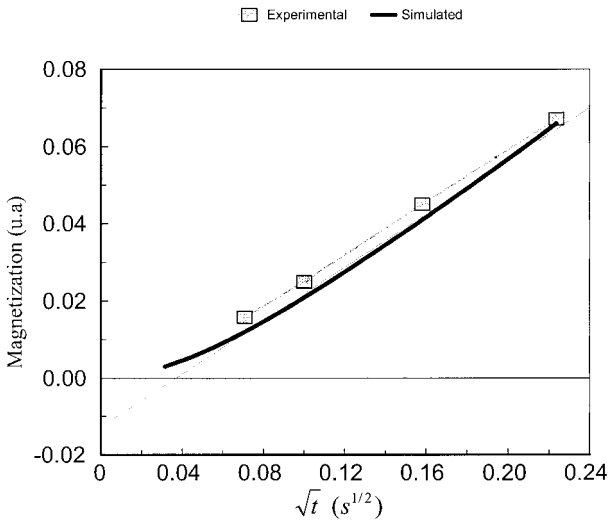

Figure 15. Adjustment of $(T_1^H)_s$ matching the computed curve and experimental points during a saturation-recovery experiment.

didate is the PS-VB16 nanocomposite. According to XRD data and TEM images, this nanocomposite is completely exfoliated.[28] The XRD data did not show any *d*-spacing following the polymerization of PS-VB16, and TEM exhibited nanodispersion of individual MMT layers (Fig. 14). On the TEM picture of Figure 14, we can see that the platelet–platelet spacing fell between 10 and 50 nm and that most of these spacings were larger than 8 nm. The VB16 curve plotted in Figure 13 shows no downward curvature, thereby implying that the sample mainly contained galleries larger than 8 nm (see our discussion in the modeling section). In our modeling, we assume a model of regular, repeating lamellar structures of alternating clay and PS. Hence, having 2.0 wt % of actual MMT (not including organic modifier), the platelet–platelet spacing is $\Delta \approx 136$ nm. This distance did not match with the MMT distance estimated by TEM (see Fig. 14). Thus, Figure 14 is a picture of a domain that has about five times the average concentration of clay; it is certainly not characteristic of the whole sample. No shear is supplied during the synthesis of the PS-VB16 sample, and the only driving force controlling the exfoliation of the sample is thermodynamic. It can then be assumed that PS-VB16 exhibits heterogeneities, that is, the distribution of the polymer–clay surface is heterogeneous. This last point is discussed in connection with T_{1l}^H.

One other opportunity we have with the VB16 sample is to estimate $(T_1^H)_s$ in our model calculation with the assumption that the clay is fully exfoliated. With the gallery spacing fixed at 136 nm, we matched the initial slope by varying $(T_1^H)_s$. A match was found for $(T_1^H)_s = 2.5$ ms (Fig. 15). We used this as a fixed parameter in all subsequent calculations related to the interpretation of T_{1l}^H.

To calculate *f*, the contribution from the intrinsic relaxation of PS must be removed before one can extract the relaxation because of the polymer–clay interface. *f* can be calculated according to eq 4

$$f = \frac{S'}{S'_{VB16}} \times \frac{R_{VB16}}{R} \tag{4}$$

where S' and S'_{VB16} are the initial slopes (corrected point by point, for the intrinsic relaxation of pure PS) of a given sample and PS-VB16, respectively; and R and R_{VB16} are the final residues determined by TGA of the given sample and PS-VB16 corresponding to the MMT concentrations in the nanocomposites. Equation 4 not only assumes that the paramagnetic character of the clays is the same (in our samples, all originate from a common MMT supplier), but there is also the assumption that all materials at the polymer–clay interface are similar in their abilities to transmit relaxation to the bulk polymer. Included in the latter statement is an assumption that none of these materials has an exceptionally high reorientational mobility for slowing down spin diffusion, nor are there large disparities in the proton densities of the organic modifiers (OMs) that lie near the clay surface. Proton densities should be comparable, judging by the structures of the OM with the possible exception of the styryltropylium cation. We did not pick up any evidence of fast reorientation at the interfaces in the Bloch decay spectra. Although there is significant expected broadening for protons in the vicinity of Fe^{3+}, it would be difficult to have rapid molecular tumbling at the interface and not see some line narrowing given the nonstoichiometric distribution of Fe^{+3}. Thus, we rationalize the use of eq 4 for these samples.

We evaluated PS and several PS/MMT nanocomposites that had been previously characterized by TEM and XRD. These PS nanocomposites incorporated different onium-salt OMs, and the different treatments led to different nanomixing. The data for deoxygenated samples are summarized in Table 1 for the 10 PS/MMT nanocompos-

Table 1. Fraction of the Interface Polymer/Clay, f, Available in PS, T_{1l}^H and XRD/TEM Characterization of Deoxygenated Model PS/MMT Nanocomposites

Polymer	Layered Silicate	*R* (wt %)	*f*	T_{1l}^H (s)	*d*-spacing from XRD (nm)	Change in *d*-spacing (nm)	TEM/XRD Conclusions
PS	—	0	0	38.58	—	—	—
—	P16			—	3.72	—	—
PS/P16	—	2.3	0.47	9.84	4.06	0.34	Well-dispersed, intercalated/ small tactoids
—	OH16			—	1.96	—	—
PS/OH16	—	2.7	0.47	14.21	3.53	1.57	Well-dispersed, intercalated/ exfoliated/small tactoids
—	VB16			—	2.87	—	—
PS/VB16	—	2.0	1.0	9.72	No peak	∞	Exfoliated
	DV		—	—	2.3	—	
PS/DV		2.3	0.61	13.02	No peak	∞	Not evenly dispersed, some exfoliation/small tactoids
—	Tropylium			—	1.55	—	—
PS/tropylium (emulsion)		2.3	0.16	31.05	No peak	∞	Poorly dispersed, large tactoids
PS/tropylium (bulk)		2.3	0.08	16.56	1.55	0	Microcomposite, large tactoids
—	MAPS				5.94		
PS/MAPS*		2.9	0.12	17.52	No peak	∞	Poorly dispersed, large tactoids
—	COPS				8.1		
PS/COPS*		2.4	0.25	14.13	6.36	−1.73	Well-dispersed intercalated/ small tactoids
—	DMHDIM			—	1.84	—	—
PS/DMHDIM		2.6	0.57	13.98		∞	Well-dispersed intercalated/ exfoliated/small tactoids
—	DMDIM			—	1.61	—	—
PS/DMDIM		3.2	0.16	29.42	1.61	0	Microcomposite, large tactoids

[a] The calculation of f considers the contribution of the relaxation of pure MAPS and COPS copolymers.

ites. This includes *f* values calculated from the initial slopes and T_{1l}^H computed by fitting (eq 1) the saturation-recovery curves and XRD/TEM characterizations. *f* covered a large range of values (between 0.08 and 1) suggesting a large difference in terms of nanomorphology for the 10 PS/MMT nanocomposites. Two different T_1^H's (only T_{1l}^H is listed for each nanocomposite sample) were obtained from biexponential fits: a short component representing from 3 to 20% of the total signal with 50 ms $< T_{1s}^H <$ 800 ms and a long component with 9 s $< T_{1l}^H <$ 39 s. The semiempirical nature of the fits and the greater emphasis on the longer T_{1l}^H has already been discussed in the previous section. Also, with two exceptions [PS-tropylium (emulsion) and PS-DMDIM], T_{1l}^H's were significantly shortened, as expected, because of the paramagnetically induced relaxation at the polymer–clay interface.

Before commenting further the data of Table 1, we offer some observations relating to the chemical stability of the OMs during nanocomposite formation; OM instability could, in principle, affect the interpretation of the data. The high shear stresses and temperatures associated with nanocomposite processing may degrade the alkyl ammonium OMs used on MMT clay during processing.[24] As an example, VanderHart et al.[24–26] detected chemical degradation of an OM, with proton Bloch decay spectra, in mechanically blended PA-6 MMT nanocomposites. We also recorded proton Bloch decay spectra at room temperature for our PS/MMT nanocomposites. Figure 16 shows a typical example of a Bloch decay spec-

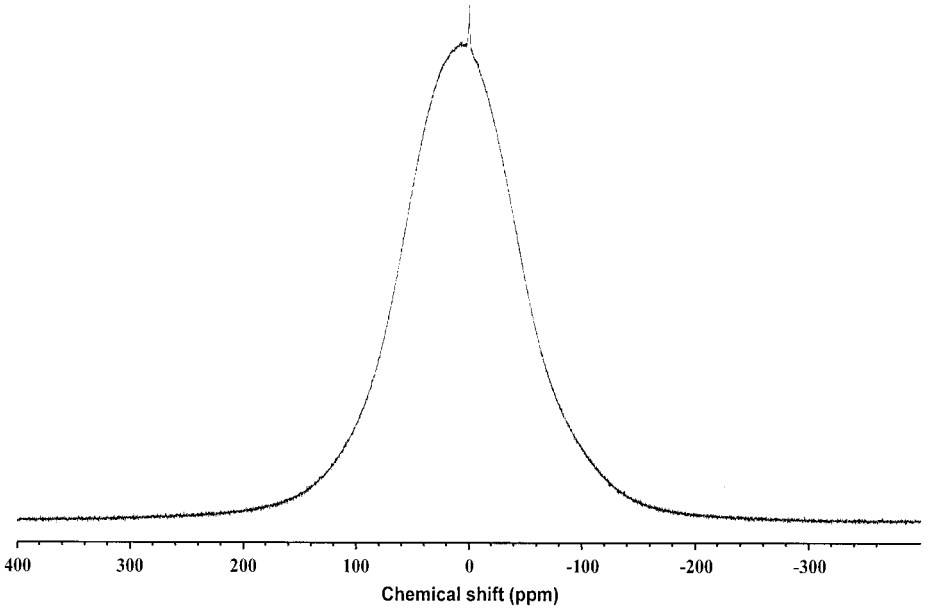

Figure 16. Typical Bloch decay spectrum recorded at room temperature and at MAS = 2.5 kHz of a PS nanocomposite.

trum of an oxygen-containing PS/MMT nanocomposite. We generally observed very small narrow lines at 0.9 and 1.3 ppm (with intensity less than 0.2% of the total intensity) on top of the 35 kHz wide PS signal. The weak intensity of the narrow lines suggested that OM degradation was not significant. Also, given that the OM degradation products reported before[24–26] in the PA-6 case were free amines that had a resonance at 2.2 ppm (aliphatic protons on carbons to the nitrogen), it was significant that we never observed this 2.2-ppm resonance. Hence, we saw no evidence of OM degradation. This result is understandable because the materials were prepared either by *in situ* polymerization (mild temperature conditions and no shear) or by extrusion where the temperature was below the degradation temperature of the OM-MMT (temperature of processing: 190 °C,

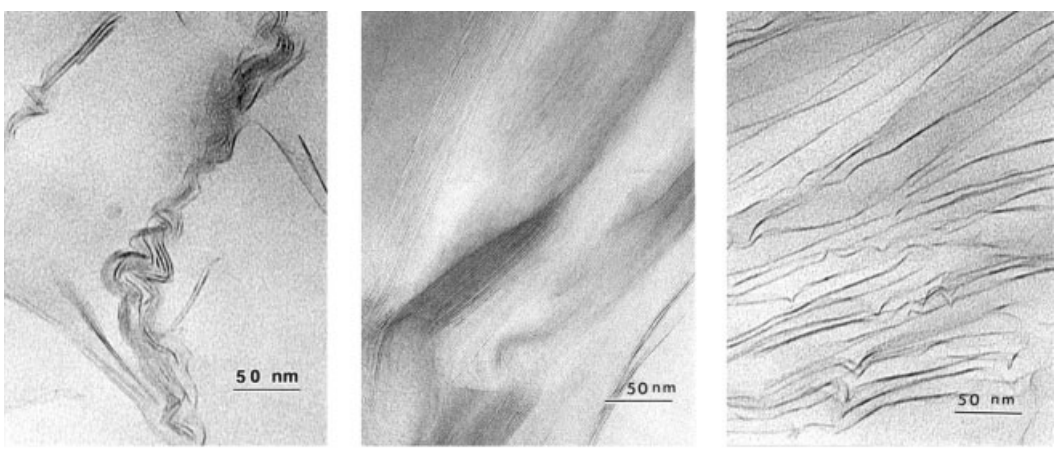

Figure 17. TEM pictures of some PS nanocomposites exhibiting three different structures: (a) intercalated, (b) mixed intercalated/exfoliated, and (c) exfoliated (from ref. 28).

50 °C below the reported temperature for OM degradation).

The data of Table 1 show how the NMR method differentiates between PS nanocomposites that range from an exfoliated to an intercalated morphology. The series PS/P16, PS/OH16, and PS/VB16 were synthesized by bulk polymerization.[28] Figure 17 shows TEM images illustrating three types of nanostructures that can be found in polymer nanocomposites, and which were observed in this series. The PS/P16, an intercalated material by TEM and XRD, has $f = 0.47$. TEM of this sample at lower magnification showed clay objects evenly spread, and at higher magnification [Fig. 17(a)] it revealed multilayer stacks (tactoids) of individual MMT layers that ranged from three layers to five layers in size. XRD indicated some intercalation with an expansion of the d-spacing by 0.34 nm upon polymerization. The lack of downward curvature in the initial slope data of Figure 13 indicated that these 3-nm galleries in the intercalated regions are, at best, a minor contributor to f. Given the overall concentration of clay in PS/P16, average spacings between fully exfoliated clay layers should be about 100 nm. In Figure 17(a), the density of platelets per unit area was about two to three times average; moreover, an f value of 0.47 seemed too high if Figure 17(a) was truly representative. We do not know whether other TEM pictures show regions with lower clay density and better separation of clay layers. This demonstrates an important difference between the NMR characterization and TEM, namely, that the NMR data are averaged over a much larger volume (ca. 0.03 cm^3) than TEM. Obtaining representative TEM images for seeing the details of clay dispersion is a statistical challenge.

PS/OH16 is a mixture of intercalated and exfoliated morphologies with $f = 0.47$. XRD data showed an expansion by 1.57 nm of the d-spacing following the polymerization. TEM of this intercalated/exfoliated sample [Fig. 17(b)] indicated good dispersion of individual MMT layers along with some tactoids that ranged from 3 layers to 10 layers in size. PS/OH16 exhibited the same f value as compared to PS/P16. As mentioned previously, we do not know whether other regions with lower clay density showed better separation of clay layers.

PS/DV was synthesized by bulk polymerization.[33] By TEM at lower magnification (not shown) this sample exhibited both clay-rich and clay-poor domains suggesting an inhomogeneous clay distribution. At higher magnification, individual platelets and small tactoids in size can be distinguished supporting the relatively high f value ($f = 0.61$).

PS/tropylium nanocomposites were synthesized both by emulsion and bulk polymerization.[30] TEM of the former sample at lower magnification (not shown) indicated that large tactoids were present and were quite evenly distributed. At higher magnification, surprisingly, multilayer stacks (tactoids) from 5 layers to 10 layers in size and individual platelets were seen. It is also rather surprising that XRD offered no evidence of a peak in the low-angle region. In this case, according to NMR the number and size of tactoids provided a relatively small polymer–clay interfacial area leading to a low value of f ($f = 0.16$). The nanocomposite synthesized by bulk polymerization exhibited, by TEM, a microcomposite structure. The polymer–clay interfacial area was again very small ($f = 0.08$) because of the presence of microparticles in the polymer. From a point of view of comparative methodologies, we can ask why TEM sees much better dispersion in the emulsion sample (at higher magnification) and why NMR provides the same ranking but rates both dispersions as poor. In this particular case, where NMR gives very small f value, the only way that one could argue for a better level of exfoliation than is deduced from the f value is that the actual clay concentration was far below that assumed, or that there was poor adhesion of the polymer at the polymer–clay surface (creating a spin-diffusion barrier in the form of, say, a physical gap). Neither of these was very plausible. As previously mentioned, tropylium is the OM with the lowest proton density. Adjusting for this feature would possibly boost both f values up by about 50% of their given values leaving the f values still low and comparable. Likewise, high reorientational mobility at the interface is not likely in one sample and not the other, especially because tropylium should participate in the polymerization. Thus, the tropylium samples were both very poorly mixed.

MAPS and COPS MMT clays (Fig. 6) were developed to foster the formation of nanocomposites by melt-blending with polymers such as poly(methyl methacrylate), PS, high-impact polystyrene, polypropylene, and polyethylene.[30] The exchange of sodium cation by a copolymer-ammonium salt on MMT should provide the compatibility of interest in the polymers mentioned previously. Molecular masses in these copolymers

were adjusted so that each molecule had about one to three cationic sites for attachment to the clay. Thus, a substantial amount of the length of each polymer was free to mix with the matrix polymer. This work only considered PS nanocomposites, but additional studies are in progress to characterize the other polymers. TEM images at lower magnification (not shown) revealed that COPS clay is well dispersed in PS but that MAPS clay is not (large agglomerates of ca. 2 μm in size). In the PS/COPS nanocomposite, it appeared that the system was intercalated by XRD and that the presence of small tactoids can also be observed in TEM images at higher magnification. In the MAPS system, clay tactoids large in size were seen. In these two particular cases, the amount of the organomodifier (MAPS or COPS salt) was about 12 wt %. Thus, we had to consider the intrinsic relaxation of MAPS and COPS in the calculation of f. The T_1^H's of deoxygenated MAPS and COPS salts were measured to be 0.74 and 2.72 s, respectively. After subtracting the contribution of MAPS and COPS salts (subtraction point by point at the earliest times), the f values became relatively small (f = 0.12 for PS/MAPS and f = 0.25 for PS/COPS). This was consistent with the presence of large tactoids in PS (PS/MAPS) or with the presence of small tactoids (PS/COPS), provided there were very few individual platelets.

The limited thermal stability of alkylammonium cations intercalated into MMT and the processing instability of some polymers such as PA-6 and PS in the presence of well-dispersed MMT had motivated the development of improved organophilic treatments for layered silicates. This need has led to the development of new thermally stable imidazolium-treated layered silicates for the preparation of nanocomposites.[12] The PS nanocomposites of the series PS/DMHDIM and PS/DMDIM used novel clays with enhanced thermal stability. Nanocomposites were prepared by extrusion.[12] DMDIM clay is poorly miscible with PS and is poorly dispersed. TEM revealed many large multilayered tactoids, with small d-spacings, and very few single-delaminated layers. In PS/DMDIM f is only 0.16. In contrast, DMHDIM clay shows much better dispersion in the PS matrix. XRD exhibited no low-angle peaks, and TEM showed some small tactoids. By NMR, f was 0.57 in this nanocomposite.

From the discussion above and from Table 1, there is a pretty strong correlation between f values above 0.5 and the loss of the XRD peak; the emulsion polymerized PS/tropylium, being an exception. Also, the correlation between larger f values and smaller T_{1l}^H values was not very strong, implying that the mere exposure of the clay surface to the polymer does not always ensure a good distribution of these exposed surfaces.

Determination of the Homogeneity of the Nanomixing

We stated in the modeling section that T_{1l}^H is a relative indicator of the homogeneity of the distribution of the actual polymer–clay interfaces in the nanocomposite. What follows is a description of the process for extracting a parameter, ϵ, that relates more directly than T_{1l}^H to this homogeneity because ϵ was normalized both for clay loading and for the f value.

Previously, we noted that when all galleries have equal spacing, the longer-time decay will be exponential, even though the early-time behavior is not exponential. When we approximate each experimental curve as a biexponential (see eq 2), then the longer time constant from that fit, T_{1l}^H, does a good job of capturing the longer-time behavior of the experimental decay. In our modeling calculation, the intrinsic relaxation times and diffusion constants were fixed for each region [recall that $(T_1^H)_s$ was fixed at 2.5 ms with the PS/VB16 initial slope] with a fixed, 0.4-nm-wide interface region. Thus, the longer-time constant was a unique function of the average spacing between clay layers. We can, therefore, compute an apparent spacing, Δ_{app}, that matches the T_{1l}^H obtained from the experimental curves. We can then compare Δ_{app} with Δ_f, the spacing in an ideally layered structure that has a surface area f times the amount expected from full exfoliation. Thus, we defined a parameter, $\epsilon = \Delta_f/\Delta_{app}$, to be a qualitative monitor of the inhomogeneity of the distribution of clay where poor homogeneity would correspond to $\epsilon \ll 1$, and good homogeneity, if our assumptions are correct, would yield $\epsilon = 1$. We recognized that ϵ is qualitative in the sense that when there is a wide distribution of Δ values, long-time exponential behavior is not expected theoretically, and Δ_{app}, obtained from an ideal layered structure with onlHy a single ϵ, may not be the most realistic estimate of the true average Δ. Therefore, one may never find a case where $\epsilon = 1$; however, relative ϵ values should relate to the homogeneity of the dispersion of surfaces included in f. A tabulation of ϵ values is found in Table 2. Clearly, it is an important assumption

Table 2. Modified Platelet–Platelet Spacing (Δ) and Estimation of the Degree of Homogeneity in PS/MMT Nanocomposites

Polymer	R (wt %)	T_{1l}^{H} (s)	f	Δ_f (nm)	Δ_{app} (nm)	ε (%)	TEM/XRD Conclusions
PS	0	38.58	0	—	—	—	—
PS/P16	2.3	9.84	0.47	252	350	72	Well-dispersed, intercalated/ small tactoids
PS/OH16	2.7	14.21	0.47	208	490	42	Well-dispersed, intercalated/ exfoliated/small tactoids
PS/VB16	2.0	9.72	1.0	136	346	39	Exfoliated
PS/DV	2.3	13.02	0.61	193	450	43	Not evenly dispersed, some exfoliation/small tactoids
PS/tropylium (emulsion)	2.3	31.05	0.16	977	$\rightarrow \infty$	$\rightarrow 0$	Poorly dispersed, large tactoids
PS/tropylium (bulk)	2.3	16.56	0.08	1504	566	266	Microcomposite, large tactoids
PS/MAPS*	2.9	17.52	0.12	127	602	21	Poorly dispersed, large tactoids
PS/COPS*	2.4	14.13	0.25	122	480	26	Well-dispersed intercalated/ small tactoids
PS/DMHDIM	2.6	13.98	0.57	183	472	39	Well-dispersed intercalated/ exfoliated/small tactoids
PS/DMDIM	3.2	29.42	0.16	470	$\rightarrow \infty$	$\rightarrow 0$	Microcomposite, large tactoids

[a] The calculation of f considers the contribution of the relaxation of pure MAPS and COPS copolymers.

that average spacings are all assumed to be proportional to the inverse of the effective clay concentration. However, because the ideal layering assumption has been made in calculating both Δ_{app} and Δ_f, sensitivity to the appropriateness of the assumption is diminished.

According to Table 2, ϵ covered a large range of values meaning that our nanocomposites ranged from homogeneous to heterogeneous. ϵ of the PS/tropylium nanocomposite prepared by bulk polymerization showed $\epsilon > 100\%$ and, strictly speaking, this did not make physical sense. As seen in the next section, this sample contained residual styrene monomer. The presence of styrene in the nanocomposite can significantly reduce T_1^H's, especially T_{1l}^H. Therefore, T_{1l}^H no longer had the meaning we attributed to it. The other PS/tropylium nanocomposite prepared by the emulsion technique had an ϵ of 0, implying very poor homogeneity. Although one might be suspicious that contaminants contribute to the shorter T_{1l}^H's, there is no corresponding ambiguity about T_{1l}^H's that approach that of pure PS unless there is high molecular mobility and consequent weak dipolar coupling for the molecules close to the polymer–clay interface. We did not see evidence for this mobility in the Bloch decay spectra. Thus, this sample had very poor clay dispersion; moreover, the suggestion is strong that the TEM picture shown in ref. 30 was definitely not representative of the whole.

PS/DMDIM similarly had $\epsilon \approx 0\%$ with a small f ($f = 0.16$), indicating that the exposed DMDIM clay was poorly dispersed in PS. This conclusion agreed with TEM (TEM pictures revealed a microcomposite structure with large tactoids) and XRD (no modification of the d-spacing of the clay).

The ϵ values for the other nanocomposites fell between 21 and 72%, suggesting that the range of dispersion for the polymer–clay interfaces was considerable. For PS/P16, ϵ was 72%, whereas for the reference material, PS/VB16, which was assumed to have complete exfoliation, ϵ was only 39%. In the TEM micrograph, Figure 17(c), the density of clay layers was unusually high, suggesting heterogeneity. Samples like PS/DMHDIM and PS/DV, which had relatively high f values ($f = 0.57$ and 0.61, respectively), also showed significant inhomogeneity ($\epsilon = 39$ and 43%, respectively). PS/COPS and PS/MAPS exhibited somewhat different behavior in the sense that they had both low f values (respectively, 0.25 and 0.12) as

Table 3. NMR, XRD, and TEM Characterizations of Oxygenated Model PS/MMT Nanocomposites

Polymer/MMT Nanocomposite	MMT Concentration (wt %)	T_t^H(ox) (τ_{null}/In2) (s)	XRD/TEM Conclusions
PS	0	1.68	—
PS/P16	2.3	1.47	Well-dispersed, intercalated/ small tactoids
PS/OH16	2.7	1.26	Well-dispersed, intercalated/ exfoliated/small tactoids
PS/VB16	2.0	1.12	Exfoliated
PS/DV	2.3	1.13	Not evenly dispersed, some exfoliation/small tactoids
PS/tropylium (emulsion)	2.3	1.36	Poorly dispersed, large tactoids
PS/tropylium (bulk)	2.3	2.07	Microcomposite, large tactoids
PS	0	1.58	—
PS/MAPS	2.9	1.32	Poorly dispersed, large tactoids
PS/COPS	2.4	1.17	Well-dispersed intercalated/ small tactoids
PS	0	1.52	—
PS/DMHDIM	2.6	1.16	Well-dispersed intercalated/ exfoliated/small tactoids
PS/DMDIM	3.2	1.38	Microcomposite, large tactoids

well as a poor dispersion of the few polymer–clay interfaces that were generated. A speculative remark about the latter samples is that when the OM was a low-molecular-weight polymer with some molecules having multiple cationic sites, there was a possibility that some of these molecules could form bridges between clay particles to resist forming galleries greater than molecular dimensions.

The two concepts of the polymer–clay interface-area fraction defined by f and the dispersion homogeneity of the polymer–clay interfaces defined by ϵ allowed us to characterize the dispersion of MMT-clay in a polymeric matrix in a more complete way. It showed us that a high polymer–clay interphase area available for dispersion in the polymer does not necessarily mean that we can also get a good distribution of the clay in the polymer, as was illustrated by the PS-VB16 nanocomposite.

T_1^H in the Presence of Oxygen

From the literature,[36,37] the adsorption of paramagnetic oxygen on aromatic polymers and in particular on PS caused a major shortening of T_1^H. The amount of adsorbed oxygen was a function of the chemical nature of PS, its molecular packing, molecular motion, and temperature. Thus, in addition to the sensitivity of T_1^H to clay dispersion, any other changes that might affect oxygen solubility or dynamics could also influence T_1^H.

When we began NMR experiments to characterize the clay dispersion, we did not recognize the very dominant role of oxygen, and we measured many samples with T_1^H, as estimated from τ_{null}, as our sole characterization parameter. We briefly include these data to illustrate the information gain with deoxygenated samples, some important pitfalls with oxygenated samples, and a fast way of estimating f, not τ_{null}, as a better, alternative approach to the characterization of oxygenated samples.

Table 3 lists the T_1^H data, obtained from τ_{null}, for our oxygen-containing PS/MMT nanocomposites. T_1^H for pure PS was dramatic, 38.6 s for deoxygenated samples, and 1.52–1.68 s for oxygenated PS. Nevertheless, T_1^H's of oxygen-containing samples, defined as T_1^H(ox), were further shortened by the paramagnetic character of the

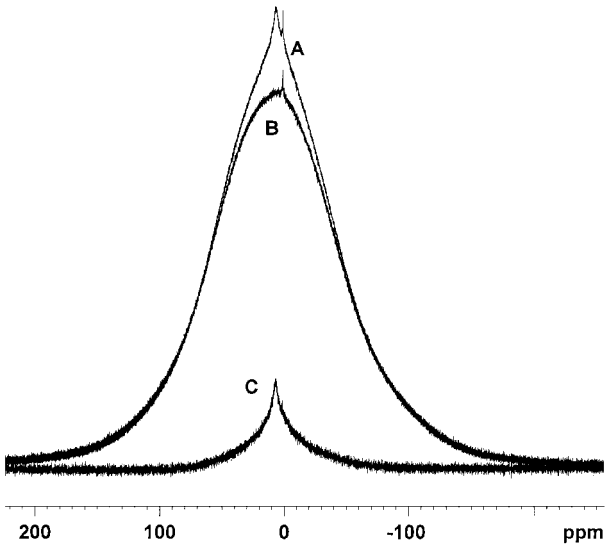

Figure 18. Bloch decay spectrum recorded at room temperature and at MAS = 2.5 kHz of the (A) PS-tropylium (bulk), (B) the PS-tropylium (bulk) baked at 130 °C *in vacuo* for 3 days, and (C) the difference between (A) and (B).

clay even if the relative effect was not nearly as large as for the deoxygenated samples.

A comparison of Tables 1–3 indicates that correlations between T_1^H(ox) and T_1^H are only modest as are correlations between larger f values and smaller T_1^H(ox) values. Of special note is the T_1^H(ox) of 2.07 s measured for PS/tropylium(bulk). An increase in T_1^H(ox) over that of bulk PS was unexpected, to say the least. We explored the reason for this increase, and on the basis of observations that followed, decided that the T_1^H(ox) increase was mainly due to the presence of unreacted styrene monomer in this sample. We decided that the likely mechanism for the increase was that the styrene monomer displaced some oxygen and weakened the contribution of oxygen to T_1^H. Observations supporting these conclusions were: (1) oxygen is so dominant in determining T_1^H(ox), (2) by high-resolution NMR, this sample had about 3% monomer by mass, and (3) the monomer showed some reorientational mobility (line narrowing) in the solid [see Fig. 18(A)]; hence, it is not expected to be an antiplasticizer[46,47] [certainly near the glass transition temperature (T_g) the monomer is a plasticizer based on a measured T_g of 85 °C for this nanocomposite vs 95 °C for pure PS], and (4) baking the sample at 130 °C *in vacuo* for 3 days [Fig. 18(B)] shows the removal of most of the mobile material [Fig. 18(C) shows the difference spectrum between the unbaked and baked sample]. Moreover, T_1^H is then reduced to 1.70 s, an almost acceptable number for a rather poorly mixed nanocomposite. This illustrates the confusion that arises when secondary issues, such as the presence of residual monomer, have their effects amplified by possibly modifying, only slightly, the solubility of oxygen. Such effects, even small ones, can cause one to draw inappropriate conclusions about the dispersion of the clay, if one does not properly consider such phenomena. In contrast, the influences of the monomer on the f and T_{1l}^H values for the deoxygenated sample do not overwhelm the conclusion of poor mixing. Depending on the intrinsic T_1^H of the monomer, the f value in Table 1 (f = 0.08) may be overestimated; however, the message of a very poor fraction is preserved. However, the monomer probably reduces T_1^H from that appropriate to the real clay distribution and that gives rise to the anomalously high ϵ of 266%.

The main message in the preceding paragraph is that use of T_1^H(ox), as measured with τ_{null}, is not a very powerful measure of clay dispersion. One could ask whether there were better approaches to gain some more reliable information about the clay dispersion from oxygenated samples, recognizing that it is fairly time-consuming to prepare deoxygenated samples. A reasonable approach, which should be more robust, is to extract that

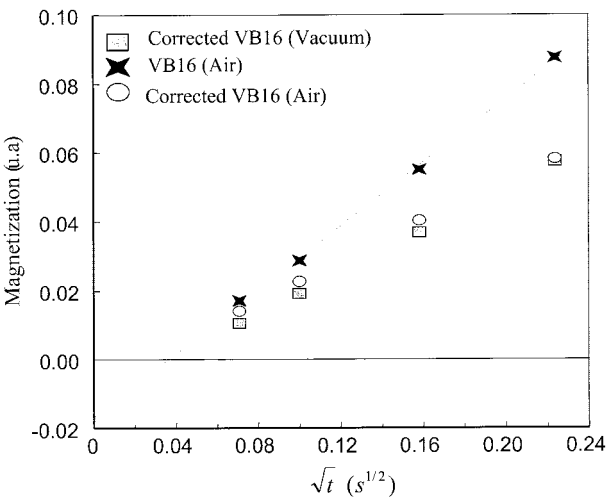

Figure 19. Magnetization from saturation-recovery experiment versus the square root of the time of oxygen containing PS-VB16 [VB16 (air)], of oxygen containing PS-VB16 corrected of the intrinsic relaxation of pure PS [corrected VB16 (air)], and of deoxygenated PS-VB16 corrected of the intrinsic relaxation of pure PS [corrected VB16 (vacuum)].

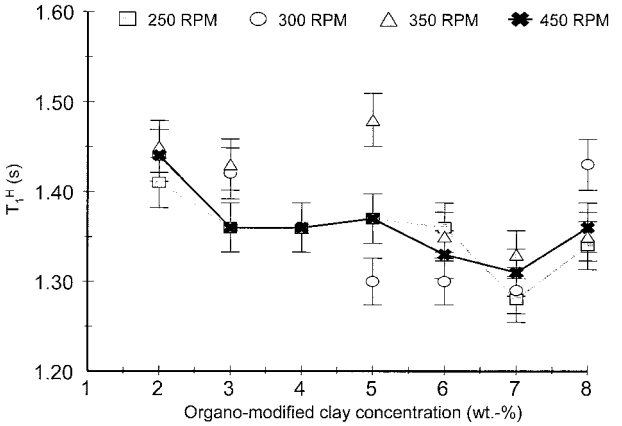

Figure 20. Evolution of T_1^H of a set of oxygen containing PS/MMT nanocomposites versus clay concentration and processing conditions.

part of the initial slope, which is due to the paramagnetic contribution. The main idea here is that because relaxation times at the polymer–clay interface (≈2.5 ms) are about two orders of magnitude faster than the fastest dipolar relaxation times (175–250 ms at 7.05 T),[45] the paramagnetic contributions are most dominant at short times where the initial slope is measured. Figure 19 illustrates this approach where for the PS/VB16 nanocomposite the experimental and T_1^H(ox) corrected initial slopes are plotted with the T_1^H corrected initial slope for the deoxygenated sample. The T_1^H(ox) and T_1^H corrections are applied, point by point, with the respective values associated with pure PS. Agreement between the two slopes was reasonably good. Therefore, if one wishes to screen samples quickly, for discarding those with low f values (good exfoliation is never accompanied by a low f value), this is a reasonable approach. As seen from the PS/VB16 sample, a good f value does not ensure that those platelets are evenly distributed. Therefore, in a screening operation one would presumably take the samples with the best f values and perform additional measurements on deoxygenated samples.

As a final comment on the use of oxygenated samples, in Figure 20 we portray the T_1^H, data obtained again from τ_{null} measurements, associated with the optimization of the mixing process in a twin-screw extruder. These data are presented with the data from a subset of deoxygenated samples, with the latter illustrating important nuances for proper interpretation of the initial slope plots. The chosen variables were clay loading (2–8 wt %) and a screw speed of 250 rpm (26.2 rad/s) to 450 rpm (47.1 rad/s). Twenty-eight samples were generated by extrusion; thus, there was considerable emphasis on rapid, or high-throughput analysis.[48–51] In fact, these samples were generated with a combinatorial approach[34] in which samples having a gradient in clay concentration are extruded. Again, this analysis predated our appreciation for the role of oxygen. The chemical uniformity of the mixed ingredients (PS and Cloisite 15A) and the uniform processing temperature make it less likely that variations in populations of small molecules would complicate interpretation as was the case for the PS/tropylium (bulk) sample just discussed. In fact, there was no NMR evidence for any degradation of the OM during processing.

All the T_1^H data in Figure 20 fell between 1.28 and 1.47 s (T_1^H of the pure PS was 1.52 s). A decrease in T_1^H with increasing MMT concentration was observed for 26 of the 28 nanocomposites. Moreover, the scatter in the data did not correlate with the screw speed. As discussed in the preceding sections, T_1^H depends on both the MMT concentration and the quality of the dispersion. T_1^H decreases noticeably for each sample as compared to the pure PS (except for the systems with 5 wt % clay and prepared at 350 rpm, and with 8 wt % clay and prepared at 300 rpm). However, this decrease was not as much as expected on the basis of analyses of nylon-6/clay composites

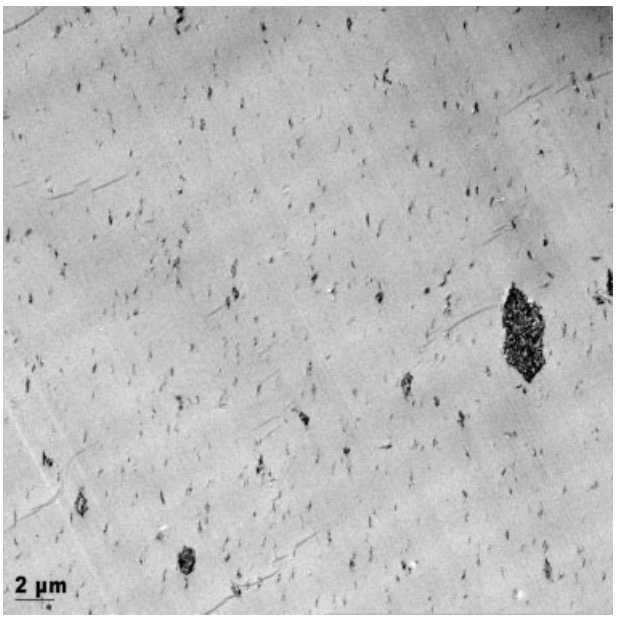

Figure 21. Low-magnification TEM of PS/MMT nanocomposite (3 wt % clay) extruded at 300 rpm.

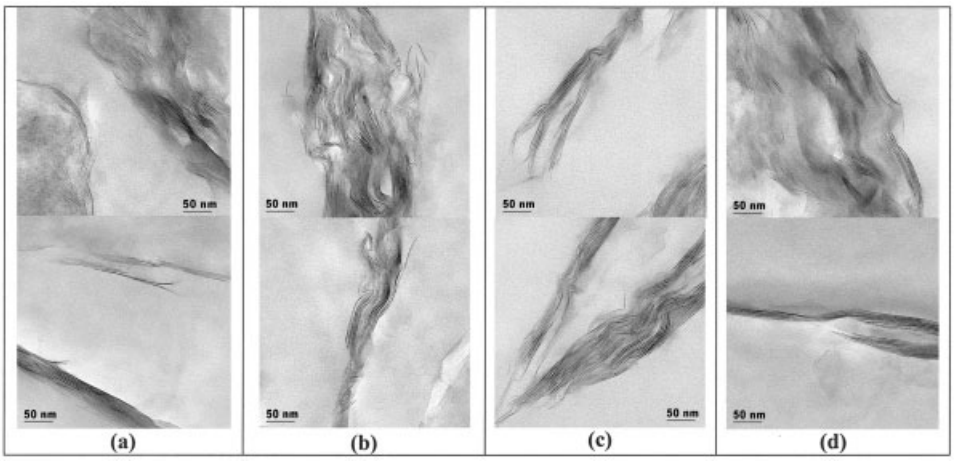

Figure 22. High-magnification TEM of PS/MMT (3 wt % organomodified MMT) extruded at (a) 250 rpm, (b) 300 rpm, (c) 350 rpm, and (d) 450 rpm.

for similar clay concentrations.[26] For example, a T_1^H of about 0.5–0.6 s, instead of the observed values (from 1.30 to 1.48 s) would be expected for good exfoliation at 5 wt % clay. Thus, by analogy the T_1^H values of these samples suggest a rather poor dispersion of the clay. A TEM image (Fig. 21), at low magnification, for a sample with 3 wt % clay and 300 rpm showed some large tactoids with smaller objects, presumed to have high clay concentration, that were rather uniformly dispersed on the scale of a few micrometers. Pairs of high-magnification images for all samples having 3 wt % clay are depicted in Figure 22. All images look quite similar. Tactoids appeared to be in the very early stages of breaking up with a very strong localization of clay layers and large spaces devoid of clay. TEM, therefore, supported the notion of poor mixing.

We also performed NMR measurements for determining f and ϵ on pure PS and the four deoxygenated samples with 3 wt % clay. Table 4 and the initial slope data are shown in Figure 23. The initial slope data resulted in f values in the range from 0.26 to 0.39, indicating modest to poor exfoliation. However, from the high-resolution TEM images, one is hard-pressed to see many gallery spacings in the range of 8 nm and above. However, the ϵ values in Table 4 are all about 0, indicating extremely poor dispersion of those polymer–clay interfaces, as is corroborated by the large regions, devoid of clay, seen by TEM. The combination of modest f values and very bad dispersion tends to suggest that the Δ distribution was very skewed toward small galleries. According to the calculations illustrated in Figure 12, galleries as small as 3 nm can make attenuated contributions to the initial slope, but their signature is a downward curvature. If we re-examine the plots in Figure 23, all of the nanocomposites have initial slopes with downward curvature verifying the prominence, at levels higher than the given f values, of galleries in the range from 3 to 7 nm. Therefore, a careful reading of these NMR data yields a specific picture of the clay dispersion

Table 4. Platelet–Platelet Spacing (Δ_{app}) and Estimation of the Degree of Homogeneity in Deoxygenated PS-Cloisite 15A Series Containing 3 wt % of Organomodified Clay and Extruded at 250, 300, 350, and 450 rpm

Polymer	Processing (rpm)	R (wt %)	T_{1l}^H (s)	f	Δ_f (nm)	Δ_{app} (nm)	ε (%)
PS	—	0	38.58	0	—	—	—
PS-Cloisite 15A-3%	250	1.7	33.35	0.39	400	$\rightarrow \infty$	$\rightarrow 0$
PS-Cloisite 15A-3%	300	1.7	34.30	0.34	468	$\rightarrow \infty$	$\rightarrow 0$
PS-Cloisite 15A-3%	350	1.7	35.75	0.26	594	$\rightarrow \infty$	$\rightarrow 0$
PS-Cloisite 15A-3%	450	1.7	33.60	0.31	509	$\rightarrow \infty$	$\rightarrow 0$

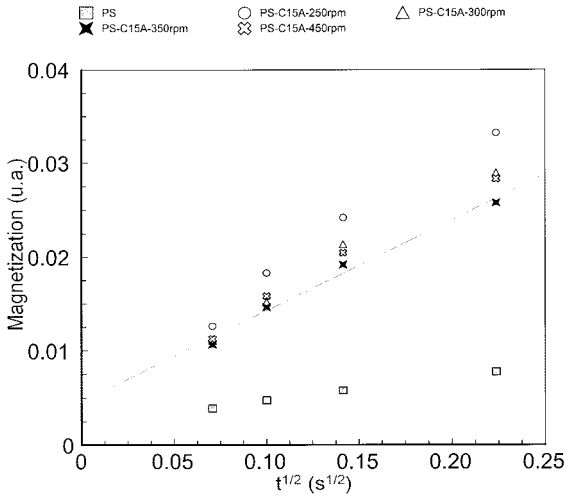

Figure 23. Magnetization from saturation-recovery experiment versus the square root of the time of deoxygenated PS/Cloisite 15A-3% nanocomposites at different screw speed (labeled PS-C15A-Xrpm).

that dovetails very well with the TEM characterization in these samples. As for the extrusion and mixing process, it seems that the energy input for breaking up tactoids is on the verge of being adequate, but is still insufficient, for the conditions chosen in these samples. The other lesson from these latter samples is that when the f value is modest, that is, in the 0.2–0.4 range, it is not necessarily true that dispersion of the polymer–clay interfaces is even. In fact, it is very important to scrutinize the initial slope data for evidence of downward curvature as a signal for small galleries and an implied very poor dispersion.

CONCLUSIONS

This work has demonstrated that solid-state NMR can be used quantitatively to characterize the degree of nanodispersion of paramagnetic MMT clay in PS matrices for samples prepared with variously modified clays with the same origin. The direct influence of the paramagnetic Fe^{3+} embedded in the aluminosilicate layers of the clay on protons within about 1.0 nm of each polymer–clay interface produces effective relaxation sinks for more distant protons. Such sinks shortened significantly proton longitudinal relaxation times. Because absorbed paramagnetic oxygen, especially in aromatic polymers, causes a shortening of T_1^H, use of deoxygenated samples greatly lengthens the intrinsic polymer T_1^H and allows one to monitor its paramagnetic contributions more thoroughly. We used a simple spin-diffusion model to calculate proton saturation-recovery curves, assuming that the nanocomposites were ideally stratified systems. On the basis of these calculations, we used proton saturation-recovery data to characterize the clay dispersion in two different ways. First, from the slope of the early-time data, between 5 and 50 ms, when plotted versus the square root of time, we get the parameter, f, which is the fraction of the total clay surface that is converted to a polymer–clay interface during composite formation. To determine f, it is assumed that the fraction of clay is known independently; it is also assumed that we have one calibration sample with a known f value. This slope, after small known corrections for relaxation, is proportional to the polymer–clay surface area over a wide range of gallery spacings, $\Delta > 10$ nm. From the long-time exponential time constant, T_{1l}^H, obtained from fitting the experimental curve, one can extract a parameter, ϵ, that relates to the homogeneity of the dispersion of the actual polymer–clay interfaces. Our approach is reasonably well correlated with the XRD and TEM data; however, there are cases in which serious questions about the representative character of available high-magnification images arise. Limitations of our method are that we need a calibrating sample; we require that MMT clays have the same paramagnetic characteristics from sample to sample, and the polymer should have not undergone any degradation nor should it have additional mobile molecules such as monomers (usually detectable in the Bloch decay spectrum) that can lead to a reduction of T_{1l}^H. Within these limitations, our method permits a detailed characterization of the nanomixing in PS/MMT materials.

We have also discussed the characterization of oxygenated samples, where sample preparation times are significantly reduced and analysis times are also shortened. Information content about the dispersion is necessarily less than for the deoxygenated samples because of the shorter times, limited by T_1^H, for following the paramagnetic contributions to T_1^H. Information is also limited by the fact that any changes that affect oxygen solubility or dynamics might also be misinterpreted as arising from clay dispersion; the presence of styrene monomer was cited as such an example. Thus, our initial approach to the characterization of clay dispersion, via a τ_{null} assessment of T_1^H for oxygenated samples, was strongly correlated with the quality of clay dispersion;

however, this assay was not very quantitative. We then illustrated a second approach, with early-time saturation-recovery data for oxygenated samples that should allow one to extract the parameter, f reasonably accurately with minimal spectrometer time. This second approach is recommended for any high-throughput analysis in which there is a premium placed on analysis time. Such an analysis represents a significant improvement in dispersion-analysis efficiency as compared with conventional methods (e.g., TEM). Moreover, this latter method uses bulk samples, conventional processing, and analytical equipment, and it results in reasonably quantitative comparisons.

Finally, we remind the reader that although this technique is applicable with spectrometers operating at fields other than the 7.05 T field used in these NMR studies, one should be prepared to find that T_1^H for the pure polymer will probably be field dependent. Moreover, a modest field dependence is also expected[25] for $(T_1^H)_s$ (in the modeling calculation) as long as the MMT clays from Southern Clay Products are used. Other clays with different Fe concentrations may have stronger field dependencies. The very long T_1^H's for deoxygenated PS are not typical for polymers; many polymers will have T_1^H's that are more than an order of magnitude shorter. Thus, the level of detail about clay dispersion that can be obtained in PS/MMT nanocomposites will not fully carry over to all polymers. However, the use of initial slopes to extract the parameter, f, will find wide applicability over different polymer systems. We note also that the strong contribution of paramagnetic oxygen to $T_1^H(ox)$ is also unusual. For example, in PA-6, going from an oxygenated to a deoxygenated sample results in a T_1^H increase of only 10%; hence, there is little advantage with deoxygenated samples. Aromatic polymers potentially have larger increases upon deoxygenation because oxygen has specific interaction with aromatic rings.

Future work will focus on expanding the NMR method to other polymer-layered silicate nanocomposites, to the characterization of degradation of the onium ion treatments on the layered silicates, and to the evaluation of domain size (nanomixing) in polymer nanocomposites on the basis of other nanoadditives (POSS, nanosilica, nanotubes, etc.).

The authors thank the following individuals for their assistance with this work: Richard Harris for help with extrusion and injection molding and Dr. Marius Murariu for the helpful discussions. The authors also thank Southern Clay Products for the donation of MMT samples and technical assistance in preparing the organically treated clays. Finally, the authors thank the following organizations for funding of this work: Federal Aviation Administration (DTFA 03-99-X-9009) and Air Force Office of Scientific Research (AFOSR-ISSA-01-0001).

REFERENCES AND NOTES

1. Alexandre, M.; Dubois, P. Mater Sci Eng 2000, 28, 1–63.
2. Kojima, Y.; Usuki, A.; Kawasumi, M.; Okada, A.; Fukushima, Y., Kurauchi, T.; Kamigaito, O. J Mater Res 1993, 8, 1185–1189.
3. Okada, A.; Fukushima, Y.; Kawasumi, M.; Inagaki, S.; Usuki, A.; Sugiyama, S.; Kurauchi, T.; Kamigaito, O. U.S. Patent 4,739,007, 1988.
4. Messersmith, P. B.; Giannelis, E. P. J Polym Sci Part A: Polym Chem 1995, 33, 1047–1057.
5. Gilman, J. W.; Kashiwagi, T.; Lichtenhan, J. D. SAMPE J 1997, 33, 40–46.
6. Gilman, J. W. Appl Clay Sci 1999, 15, 31–49.
7. Usuki, A.; Kojima, Y.; Kawasumi, M.; Okada, A.; Fukushima, Y.; Kurauchi, T.; Kamigaito, O. J Mater Res 1993, 8, 1179–1184.
8. Messersmith, P. B.; Giannelis, E. P. Chem Mater 1994, 6, 1719–1725.
9. Wang, M. S.; Pinnavaia, T. J Chem Mater 1994, 6, 468–474.
10. Zhu, J.; Wilkie, C. A. Polym Int 2000, 49, 1158–1163.
11. Jeon, H. G.; Jung, H. T.; Lee, S. D.; Hudson, S. Polym Bull 1998, 41, 107–113.
12. Gilman, J. W.; Awad, W. H.; Davies, R. D.; Shields, J.; Harris, R. H.; Davis, C.; Morgan, A. B.; Sutto, T. E.; Callahan, J.; Trulove, P. C.; DeLong, H. C. Chem Mater 2002, 14, 3776–3785.
13. Giannelis, E. Adv Mater 1996, 8, 29–39.
14. Gilman, J. W.; Kashiwagi, T.; Giannelis, E. P.; Manias, E.; Lomakin, S.; Lichtenhan, J. D.; Jones, P. Fire Retardancy of Polymers - The Use of Intumescence; Le Bras, M.; Camino, G.; Bourbigot, S.; Delobel, Eds.; The Royal Society of Chemistry: Cambridge, 1998; pp 223–235.
15. Gilman, J. W.; Jakson, C. L.; Morgan, A. B.; Harris, R. H.; Manias, E.; Giannelis, E. P.; Wuthenow, M.; Hilton, D.; Philips, S. H. Chem Mater 2000, 12, 1866–1873.
16. Devaux, E.; Bourbigot, S.; El Achari, A. J Appl Polym Sci 2002, 86, 2416–2423.
17. Lan, T.; Kaviratna, P. D.; Pinnavaia, T. J Chem Mater 1994, 6, 573–575.
18. Sugahara, Y.; Sugiyama, T.; Nagayama, T.; Kuroda, K.; Kato, C. J Ceram Soc Jpn 1992, 100, 413–416.

19. Vaia, R. A.; Ishii, H.; Giannelis, E. P. Chem Mater 1993, 5, 1694–1696.
20. Morgan, A. B.; Gilman, J. W. J Appl Polym Sci 2003, 87, 1329–1338.
21. Lincoln, D. M.; Vaia, R.; Wang, Z. G.; Hsiao, B. S. Polymer 2001, 42, 1621–1631.
22. Hyun, Y. H.; Lim, S. T.; Choi, H. J.; Jhon, M. S. Macromolecules 2001, 34, 8084–8093.
23. Krishnamoorti, R.; Vaia, R. A.; Giannelis, E. P. Chem Mater 1996, 8, 1728–1734.
24. VanderHart, D. L.; Asano, A.; Gilman, J. W. Macromolecules 2001, 34, 3819–3822.
25. VanderHart, D. L.; Asano, A.; Gilman, J. W. Chem Mater 2001, 13, 3781–3795.
26. VanderHart, D. L.; Asano, A.; Gilman, J. W. Chem Mater 2001, 13, 3796–3809.
27. Wagner, D. Kunstoffe 2002, 92, 17–19.
28. Zhu, J.; Morgan, A. B.; Lamelas, F. J.; Wilkie, C. A. Chem Mater 2001, 13, 3774–3780.
29. Zhang, J.; Wilkie, C. A. Polym Degrad Stab, in press.
30. Su, S.; Jiang, D.; Wilkie, C. A. Polym Degrad Stab, in press.
31. Wang, D.; Zhu, J.; Yao, Q.; Wilkie, C. A. Chem Mater 2002, 14, 3837–3843.
32. Zhu, J.; Uhl, F. M.; Morgan, A. B.; Wilkie, C. A. Chem Mater 2001, 13, 4649–4654.
33. Su, S.; Wilkie, C. A. J Polym Sci Part A: Polym Chem 2003, 41, 1124–1135.
34. Gilman, J. W.; Bourbigot, S.; Shields, J. R.; Nyden, M.; Kashiwagi, T.; Davis, R. D.; VanderHart, D. L.; Demory, W.; Wilkie, C. A.; Morgan, A. B.; Lyon, R. E. Proceedings of SAMPE 2003, May 2003, Long Beach, CA.
35. Ryan, L. M.; Taylor, R. E.; Paff, A. J.; Gerstein, B. C. J Chem Phys 1980, 72, 508–515.
36. Capitani, D.; De Rosa, C.; Ferrando, A.; Grassi, A.; Segre, A. L. Macromolecules 1992, 25, 3874–3880.
37. Capitani, D.; Segre, A. L.; Blicharski, J. S. Macromolecules 1995, 28, 1121–1128.
38. Farrar, T. C.; Becker, E. D. Pulse and Fourier Transform NMR; Academic: New York, 1971; p 20.
39. Kirk-Othmer Encyclopedia of Chemical Technology, 4th ed.; Kroschurtz, J. S., Ed.; Wiley: New York, 1993; Vol. 6.
40. Blumberg, W. E. Phys Rev 1960, 119, 79–88.
41. Abragam, A. The Principles of Nuclear Magnetism; Oxford University Press: London, 1961; Chapter V.
42. VanderHart, D. L.; McFadden, G. B. Solid State Magn Nucl Res 1996, 7, 45–66.
43. Clauss, J.; Schmidt-Rohr, K.; Spiess, H. W. Acta Polym 1993, 44, 1–17.
44. Crank, J. The Mathematic of Diffusion; Oxford University Press: London, 1957.
45. Abragam, A. The Principles of Nuclear Magnetism; Oxford University Press: London, 1961; Chapter VIII.
46. Duda, J. L.; Romdhane, I. H.; Danner, R. P. J Non-Cryst Solids 1994, 172, 715–720.
47. Anderson, S. L.; Grulke, E. A.; DeLassus, P. T.; Smith, P. B.; Kocher, C. W.; Landes, B. G. Macromolecules 1995, 28, 2944–2954.
48. Brocchini, S.; James, K.; Tangpasuthadol, V.; Kohn, J. J Am Chem Soc 1997, 119, 4553–4554.
49. Meredith, J. C.; Karim, A.; Amis, E. Macromolecules 2000, 33, 5760–5762.
50. Smith, A. P.; Douglas, J. F.; Meredith, J. C.; Amis, E. J.; Karim, A. J Polym Sci Part B: Polym Phys 2001, 39, 2141–2158.
51. Karim, A.; Yurekli, K.; Meredith, J. C.; Amis, E.; Krishnamoorti, R. Polym Eng Sci 2002, 42, 1836–1848.